Paper published in:

M.A. Al-Sharrad, D. Gallipoli, S.J. Wheeler (2017).

Experimental investigation of evolving anisotropy in unsaturated soils.

Géotechnique, 67(12): 1033–1049

http://dx.doi.org/10.1680/jgeot.15.P.279

EXPERIMENTAL INVESTIGATION OF EVOLVING ANISOTROPY IN UNSATURATED SOILS

Muayad A. Al-Sharrad[1], Domenico Gallipoli[2], Simon J. Wheeler[3]

[1] Lecturer, Department of Civil Engineering, College of Engineering, University of Anbar, Iraq (formerly School of Engineering, University of Glasgow, Glasgow, UK)
email: an_mission@yahoo.com

[2] Professor, Laboratoire SIAME, Université de Pau et des Pays de l'Adour, Anglet, France (formerly School of Engineering, University of Glasgow, Glasgow, UK)
email: domenico.gallipoli@univ-pau.fr

[3] Professor, School of Engineering, University of Glasgow, Glasgow, UK
email: simon.wheeler@glasgow.ac.uk

DATE OF SUBMISSION: 01 - 2017

NUMBER OF WORDS: 6992

NUMBER OF TABLES: 3

NUMBER OF FIGURES: 21

CORRESPONDING AUTHOR: Dr Muayad A. Al-Sharrad

198/4/257
New Erbil
Erbil 44001
Iraq
e-mail: an_mission@yahoo.com

ABSTRACT: This paper investigates the "initial" and "evolving" mechanical anisotropy of a compacted unsaturated soil. A wide campaign of triaxial compression and extension tests, involving different stress and suction paths, has been performed on both isotropically and anisotropically compacted samples of unsaturated Speswhite Kaolin. The first objective is the definition of the initial yield surface of the compacted soil after suction equalization and before any plastic loading/wetting path takes place. This is followed by the investigation of the evolution of the yield surface induced by plastic straining along different loading/wetting paths. Experimental results are interpreted by using two alternative stress variables, namely net stresses σ_{ij} and Bishop's stress $\sigma_{ij}^*=\sigma_{ij}+\delta_{ij}\,S_r s$ (where δ_{ij} is Kronecker delta, S_r is the degree of saturation and s is suction). Constant suction cross-sections of the yield surface are represented as distorted ellipses not passing through the origin in the q:p plane of deviator stress versus mean net stress, and by distorted ellipses passing through the origin in the q:p^* plane of deviator stress versus mean Bishop's stress. The inclination of these distorted elliptical yield curves evolves with plastic straining but remains the same at all suction levels for a given level of plastic deformation. The critical state lines in the planes q:p and q:p^*, or in the semi-logarithmic v:ln$p$ and v:lnp^* planes (v is the specific volume), are generally independent of initial anisotropy or stress history, suggesting that fabric memory tends to be erased at critical state.

KEYWORDS: soil anisotropy, fabric orientation, soil compaction, laboratory testing, clays, critical state, elasto-plastic behaviour, unsaturated soils, partial saturation, suction, constitutive relations

LIST OF NOTATIONS

δ_{ij}	Kronecker delta
σ_{ij}	net stress tensor
σ_{ij}^*	Bishop's stress tensor
$[\Delta q/\Delta p]$	net stress increment ratio
$[\Delta q/\Delta p']$	effective stress increment ratio
B	ratio of pore water pressure increase to cell pressure increase for saturated triaxial tests
G	shear modulus
m	aspect ratio of the distorted elliptical yield curve in the q:p plane
M	slope of the critical state line in the q:p plane
m^*	aspect ratio of the distorted elliptical yield curve in the q:p^* plane
M^*	slope of the critical state line in the q:p^* plane
m_c	aspect ratio of the yield curve in the q:p plane for $q/(p+p_s(s))>\alpha$
m_c^*	aspect ratio of the yield curve in the q:p^* plane for $q/p^*>\alpha^*$
m_e	aspect ratio of the yield curve in the q:p plane for $q/(p+p_s(s))<\alpha$

m_e^*	aspect ratio of the yield curve in the q:p^* plane for $q/p^* < \alpha^*$
p	mean net stress
p^*	mean Bishop's stress
p'	mean effective stress
p_{atm}	atmospheric pressure
p_m	size of the distorted elliptical yield curve in the q:p plane
p_m^*	size of the distorted elliptical yield curve in the q:p^* plane
$p_s(s)$	intercept of the compression and extension critical state lines at suction s in the q:p plane
q	deviator stress
s	matric suction
S_r	degree of saturation
v	specific volume
α	inclination of the distorted elliptical yield curve in the q:p plane
α^*	inclination of the distorted elliptical yield curve in the q:p^* plane
$\Gamma(s)$	intercept of the critical state lines at suction s in the v:ln p plane
$\Gamma^*(s)$	intercept of the critical state lines at suction s in the v:ln p^* plane
ε_s	shear strain (calculated as 2/3 of axial strain minus radial strain)
η	net stress ratio in the q:p plane
η^*	net stress ratio in the q:p^* plane
κ^*	gradient of elastic compression/swelling line in the v:ln p^* plane
κ_s	gradient of elastic compression/swelling line in the v:ln (s+p_{atm}) plane
$\psi(s)$	gradient of the critical state lines at suction s in the v:ln p plane
$\psi^*(s)$	gradient of the critical state lines at suction s in the v:ln p^* plane

1. Introduction

Soils can exhibit an orientated fabric which results in anisotropic properties such as the dependency of deformation on loading direction and the dependency of permeability on flow direction. Anisotropic properties are found in both natural clays and engineered fills as a consequence of the processes of deposition and compaction, respectively. This initial anisotropy can be altered by rearrangement/reorientation of particles due to plastic deformation, a phenomenon referred to as "evolving" or "induced" anisotropy. Even an initially isotropic soil can therefore develop anisotropic properties if plastically loaded along a deviatoric stress path.

At microscopic level, the anisotropy of soils has been studied by scanning electron microscopy (SEM). For example, Hattab and Fleureau (2011) and Hicher *et al.* (2000) presented a microstructural analysis of saturated Kaolin specimens prepared from slurry. They found that isotropically consolidated specimens show an aggregated fabric with edge-to-face particle associations and no preferential orientation. One-dimensionally consolidated samples show instead an anisotropic fabric with preferential particle orientation perpendicular to the direction of loading and face-to-face particle associations which results in smaller pore sizes. Close to critical state, soils exhibit an oriented fabric along the direction of shearing with face-to-face particle arrangements.

Past laboratory research has focused on the mechanical anisotropy of saturated soils with a smaller number of investigations regarding unsaturated soils. These studies have shown that anisotropic soils exhibit: a) an inclined yield curve in the plane of deviator stress versus mean stress (e.g. Graham *et al.*, 1983; Cui and Delage, 1996; Della Vecchia *et al*., 2012), b) occurrence of shear strains even during isotropic loading or wetting (e.g. Zakaria *et al*., 1995) and c) a dependency of normal compression behavior on degree of anisotropy (e.g. Sivakumar *et al*., 2010a and 2010b).

Specimens with isotropic fabric have been usually prepared by static compaction with an all-round pressure (see, for example, Sivakumar, 2005) while specimens with anisotropic fabric have been usually prepared by one-dimensional compaction inside a stiff-walled mould (Sivakumar, 1993; Cui and Delage, 1996; Sharma, 1998; Wheeler and Sivakumar, 2000). This is slightly different from the present work where anisotropic specimens were statically compacted by application of a deviatoric path with simultaneous control of axial and radial stresses.

Cui and Delage (1996) conducted suction-controlled triaxial tests on one-dimensionally compacted silt samples subjected to isotropic loading followed by probing at different stress ratios in triaxial compression. They proposed an anisotropic unsaturated elasto-plastic model where constant suction cross-sections of the yield locus have the form of rotated ellipses in the q:p plane of deviator stress versus mean net stress. This investigation was however

limited to compaction-induced anisotropy and did not explore the rotation of the constant suction yield ellipses caused by the evolution of fabric anisotropy with plastic straining.

Romero *et al.* (2003) observed that that the ratio between shear and axial strain changed from an initially negative value to one during wetting of anisotropic specimens subjected to a constant isotropic load. This observation was explained with the occurrence of plastic deformations which, under isotropic loading, progressively reduce the degree of fabric anisotropy. Romero *et al.* (2003) interpreted their findings in terms of an elastoplastic hardening framework where changes of fabric anisotropy were linked to plastic strains but without formalizing the corresponding evolution of the yield locus.

This paper presents an experimental investigation of the yielding and critical state behaviour of isotropically and anisotropically compacted Speswhite Kaolin specimens under unsaturated conditions. Likewise other works on compacted soils, the adopted sample preparation technique produces a highly collapsible material with an open fabric which is closer to the fabric of engineered fills rather than natural soils. A wide campaign of suction controlled triaxial tests, in both compression and extension, has been performed to explore the changes of anisotropy induced by plastic straining. Test results are interpreted by using two alternative stress variables, namely the net stresses σ_{ij} and the Bishop's stresses $\sigma_{ij}^* = \sigma_{ij} + \delta_{ij} S_r s$ (where δ_{ij} is Kronecker delta, S_r is degree of saturation and s is suction). Bishop's stress σ_{ij}^* has the advantage of naturally reducing to Terzaghi effective stress when degree of saturation becomes equal to one.

2. Experimental methods

Specimens preparation

Specimens with isotropic or anisotropic fabrics were produced by subjecting the soil to different static compaction stress paths as described in the following. Speswhite Kaolin was first mixed at a water content of 25% and passed through a 2 mm sieve before being sealed inside plastic bags at constant temperature to allow moisture homogenization for one day. A water content of 25% was chosen for consistency with previous works on unsaturated Speswhite Kaolin (e.g. Sivakumar, 1993 and Raveendiraraj, 2009). After moisture homogenization, the soil mix was placed inside a latex membrane in a conventional triaxial cell and then isotropically loaded, with the pore drainage line open to atmosphere, to a mean net stress of p=100 kPa before being unloaded back to zero. This preliminary loading-unloading path had the purpose of ensuring that the subsequent static compaction stress path (performed in the same triaxial cell) started from an identical soil state. The static compaction process consisted in the application of a mean net stress of p=250 kPa along either an isotropic path, i.e. with a net stress ratio $\eta = q/p = 0$ (method A), or along an anisotropic path, i.e. with a net stress ratio $\eta = q/p \approx 1.2$ (method B). In both

cases, pore air was allowed to drain to atmosphere throughout the loading process. In spite of the relatively high stress ratio of the anisotropic compaction path, the soil remained far from critical state due to the relative high cohesion generated by the partially saturated condition. This was confirmed by the absence of any shear plane on the sample surface.

Two additional samples, one isotropic and one anisotropic, were similarly compacted inside a "double-walled" triaxial cell (instead of a conventional triaxial cell as described above) to measure the change of specific volume during the compaction stress path. Interestingly, the specific volume was significantly higher for the isotropically compacted sample than for the anisotropically compacted one (Fig. 1), despite both isotropic and anisotropic samples were compacted to the same mean net stress p=250 kPa. This suggests that an anisotropic compaction stress state will produce denser samples than an isotropic one for the same mean stress level.

The compacted samples had an approximate diameter of 90 mm and height of 140 mm. Smaller triaxial specimens of 50 mm diameter were then cored along the vertical direction and trimmed inside a split mould to a height of 100 mm, with the exception of the specimens subjected to triaxial extension which were trimmed to a smaller height of 75 mm. This shorter height was necessary to allow enough travel of the loading piston inside the triaxial cell upon extension. Bishop and Henkel (1962) state that the slenderness ratio of triaxial specimens should be between 1.5 and 2.5, which agrees with the dimensions of all specimens tested in the present work.

This stress-controlled compaction method produced isotropic and anisotropic specimens that were homogeneous, stiff enough for handling and repeatable in terms of void ratio and water content (means and standard deviations of the main properties after compaction are given in Table 1). Additional information regarding the specimen preparation procedure can be found in Al-Sharrad *et al*. (2012) and Al-Sharrad (2013).

Stress paths

Three independent triaxial systems were used in the present study. System 1 and System 2 were double-walled stress-path cells, with a glass inner wall, for suction-controlled compression and extension tests on unsaturated specimens. System 3 was instead a conventional triaxial cell for compression and extension tests on saturated specimens.

The aim of the testing programme was to determine:

a) the "initial" yield curves after equalization under a nominal stress state at the three suctions of zero (corresponding to saturated conditions), 100 kPa or 300 kPa;

b) the "evolved" yield curves after plastic deformation produced by loading at the same suction levels mentioned in the point above.

The suction of the as-compacted specimens was about 650 kPa, as measured by the axis-translation technique. This suction level was too high to determine the corresponding yield curve by means of the available equipment. Nevertheless, the change of anisotropy during the subsequent equalization at lower suctions was considered negligible as inferred from the occurrence of very small deformations (see later for further details).

The entire experimental programme consisted of 11 test series. Each series had the objective of identifying one yield curve at constant suction and therefore required between 5 and 7 "probing" tests along different triaxial compression/extension paths to obtain between 5 and 7 distinct yield points. In the test series investigating the initial yield curves, specimens were probed by loading along different linear paths from the nominal stress level imposed during equalization until a final state well beyond yielding. Unsaturated specimens were loaded at a constant ratio of net stress increments [$\Delta q/\Delta p$] while saturated specimens were loaded at a constant ratio of effective stress increments [$\Delta q/\Delta p'$]. In the test series investigating the evolved yield curves, an intermediate plastic stage was introduced between the end of equalization and the start of probing. The objective of this intermediate stage was the generation of plastic deformations by means of a loading-unloading path which produced the desired evolution of yield surface.

Each test series is identified by a code beginning with either A, for isotropically compacted specimens, or B, for anisotropically compacted specimens. The test series investigating the evolution of anisotropy by means of an intermediate plastic deformation stage include an additional lowercase letter (i.e. a, b, c or d) that describes the nature of the intermediate plastic stage. Finally, all series codes include a number that indicates the constant suction at which the probing paths were conducted. Individual tests are identified by the corresponding series code followed by a number in brackets indicating the probing stress ratio. For instance, A300(1) is the code of a test performed on an isotropically compacted sample at a suction s=300 kPa with a probing net stress ratio [$\Delta q/\Delta p$] =1.

A summary of all test series is provided below:

- Test series A0, A100 and A300 investigate the initial yield curves of isotropically compacted specimens after equalization at s=0, 100 and 300 kPa while test series B0, B100 and B300 investigate the initial yield curves of anisotropically compacted specimens at the same suctions. Each series includes seven tests with probing net stress ratios [$\Delta q/\Delta p$] (or effective stress ratios [$\Delta q/\Delta p'$] for saturated tests) of 3, 2, 1, 0, -0.5, -1 and -1.5 (Fig. 2).

- Test series B100bis investigates the behavior of specimens that were anisotropically compacted to a lower mean net stress (i.e. p=160 kPa instead of p=250 kPa) to obtain a larger specific volume that is similar to that of isotropically compacted specimens. This series includes six tests performed at s=100 kPa with probing net stress ratios of 2, 1, 0, -0.5, -1 and -1.5 (Fig. 2).

- Test series Ba300, Bb300 and Bc300 investigate the evolved yield surfaces of the anisotropically compacted specimens subjected to three different intermediate plastic paths at s=300 kPa. Figs. 3, 4 and 5 show the probing ratios of each series, which are equal to (0.5, 0, -0.5, -1, -1.5), (1.2, 0.5, -0.5, -1, -1.5) and (1.2, 0.5, 0, -0.5, -1.5), respectively. The probing ratios are different for the three series because each set does not include the ratio of the corresponding plastic path. For this particular ratio, probing is not necessary because the yield point is already known and coincides with the pre-consolidation stress at the end of the plastic path. The plastic paths of the three series consist in a loading–unloading, between the equalization stress state and a mean net stress p=200 kPa, with stress ratios of 1.2, 0 and -1, respectively (see dashed lines in Figs. 3, 4 and 5). The value p=200 kPa is 1.7 times larger than the average yield mean net stress measured in series B300 during the three probing paths with similar stress ratios of 1, 0 and -1. It is therefore large enough to generate significant irreversible deformations with a consequent evolution of the yield surface. But it is also small enough to remain far from critical state even at the highest stress ratios of 1.2.

- Test series Bd100 investigates the evolution of the yield surface of anisotropically compacted specimens subjected to plastic wetting under a relatively high isotropic load. As shown in Fig. 6, specimens were first loaded at s=300 kPa from the nominal stress state after equalization to p=90 kPa with a stress ratio of zero. Plastic deformations were subsequently induced by wetting under a constant stress state from s=300 kPa to s=100 kPa. Specimens were then unloaded before being probed at s=100 kPa with net stress ratios of 1.2, 0.5, -0.5, -1 and -1.5 (Fig. 7).

The probing paths with the steepest stress ratios of 3, 2, 1, 1.2, -1 and -1.5 were performed under strain-controlled conditions until critical state was attained by imposing a constant axial displacement rate of 0.2 mm/hr while adjusting the radial stress to maintain the required stress ratio. Conversely, the probing paths with the shallowest ratios of 0.5, 0 and -0.5 were performed under stress-controlled conditions by increasing the radial stress at a constant rate of 2 kPa/hr while adjusting the deviator stress to maintain the required stress ratio. This loading rate was slow enough to ensure drained conditions as confirmed by the negligible volume changes observed during a 24 hours rest period after loading at different suctions. The above rates resulted in similar durations for both strain-controlled and stress-controlled paths. The shallowest ratios of 0.5, 0 and -0.5 would never attain critical state and were therefore followed by shearing to failure in compression or extension at constant cell pressure by imposing a

constant axial displacement rate of 0.2 mm/hr (the final shearing stages are marked by letters *c*, *d* and *e* in Figs. 2, 3, 4, 5 and 7).

The reliability of results was investigated by repeating tests on ostensibly identical specimens under both saturated and unsaturated conditions, which confirmed the repeatability of the testing procedure (Al-Sharrad, 2013).

3. Test results

Suction equalization and saturation stages

During equalization, suction was imposed at the top and bottom extremities of the specimens under a constant nominal net stress state of p=12 kPa, q=6 kPa (for tests involving triaxial compression) or p=10 kPa, q=0 (for tests involving triaxial extension). Fig. 8 presents the variation of water content and specific volume during typical equalization stages at s=300 kPa and s=100 kPa for both isotropically and anisotropically compacted samples. Equalization lasted between 3 and 6 days, during which water content and specific volume continuously increased (resulting in an increase of degree of saturation) without any plastic collapse. The increase of moisture content was almost identical for isotropically and anisotropically compacted specimens while the increase of specific volume was sometimes slightly higher for isotropically compacted specimens and sometimes slightly higher for anisotropically compacted specimens.

Equalization at zero suction (i.e. saturation) consisted of a two-step process. In the first step, specimens were subjected to a confining pressure of 10 kPa while water was flushed through them by imposing a pore pressure of 8 kPa at the base and atmospheric pressure at the top, until no air bubbles were detected in the top drainage line (usually after 2-3 days). During the second step, cell and pore water pressures were simultaneously increased to 305 kPa and 300 kPa, respectively, at a rate of 4 kPa/hr to dissolve any remaining air pocket inside the pores. After this, the B value was calculated between 0.97 and 0.99, which indicated good saturation. The effective stress applied to the specimens during saturation was low enough to avoid any plastic collapse.

The average properties and corresponding standard deviations after equalization of isotropically and anisotropically compacted specimens are given in Table 1. In each test series, all specimens attained very similar conditions after equalization, which emphasizes the repeatability of the adopted sample preparation procedure.

Probing and shearing of specimens after equalization

Fig. 9 compares the probing stages at s=300 kPa of three isotropically compacted specimens from series A300 and three anisotropically compacted specimens from series B300. The probing stress ratio of the three tests are $[\Delta q/\Delta p]$=1 (Figs. 9(a,b,c,d)), $[\Delta q/\Delta p]$=0 (Figs. 9(e,f,g,h)) and $[\Delta q/\Delta p]$=-1 (Figs. 9(i,j,k,l)). Figs. 9(e,f,g,h) also

include the results from the final shearing stage at the end of probing with $[\Delta q/\Delta p]=0$. Inspection of Figs. 9(a,i) indicates that, during probing at net stress ratios of 1 and -1, the initial stiffness is higher for the anisotropically compacted specimens compared to the isotropically compacted ones, probably because of the lower initial void ratio and oriented fabric of the former specimens. However, as loading advances, memory of compaction is gradually erased and the stiffness becomes increasingly similar.

Fig. 9(e) shows that, during probing at $[\Delta q/\Delta p]=0$, isotropically compacted specimens exhibit a small positive shear strains while anisotropically compacted specimens exhibit a small negative shear strain. The development of shear strains might seem surprising given the isotropic nature of the probing path but it is explained by the little deviatoric component of the initial stress state corresponding to the end of the previous equalization stage (p=12 kPa, q=6 kPa). Another reason, which only applies to anisotropically compacted specimens, is the orientation of soil fabric that results in the development of shear strains even under isotropic loads. During subsequent shearing to critical state, isotropically and anisotropically compacted specimens show similar mechanical responses, which indicates that the previous probing path at $[\Delta q/\Delta p]=0$ has induced similar fabrics in both materials.

All tests attain a peak deviator stress that corresponds to the formation of a shear band, as confirmed by visual inspection of specimens (Figs. 9(a,e,i)). Post-peak results are presented just for completeness but, after strain localization, measurements of stresses and deformations become inaccurate and no conclusions can be drawn from the data. The tests shown in Figs. 9(a,e,i), as well as other tests not presented here (see Al-Sharrad, 2013), indicate that the isotropically and anisotropically compacted specimens attain similar values of peak deviator stress when subjected to the same shearing path. However, the shear strains at peak were larger for the isotropically compacted specimens than for anisotropically compacted ones. This is probably because of the random particle arrangement of isotropically compacted specimens, which requires larger strains to produce a fabric rearrangement parallel to the shear plane. This hypothesis requires however further experimental validation.

Figs. 9(b,f,j) show contractant behaviour for all specimens, with a progressive stabilization of specific volume as the peak is approached. Figs. 9(c,g,k) compare the volumetric behaviour in terms of mean net stress and mean Bishop's stress in the v:ln$p$ and v:ln p* planes, respectively. The initial difference in specific volume between anisotropically and isotropically compacted specimens decreases as loading progresses and fabric memory is erased by cumulative plastic deformations.

Figs. 9(d,h,l) show that degree of saturation S_r increases during all tests due to a reduction in specific volume at approximately constant water content. Therefore, the initial difference in degree of saturation between

isotropically and anisotropically compacted specimens reduces as loading progresses in a similar fashion to the reduction of the difference in specific volume.

Fig. 10 compares the response of isotropically compacted samples during loading at different suctions along the two ratios of 1 and -1 which are symmetrical about the hydrostatic axis. Three triaxial compression tests A300(1), A100(1) and A0(1) (sample slenderness ratio of 2) are compared with the corresponding triaxial extension tests A300(-1), A100(-1) and A0(-1) (sample slenderness ratio of 1.5). The negative values of deviator stress and shear strains during triaxial extension are plotted as absolute values to facilitate comparison. The evolution of plastic strains is similar for both stress ratios, though the extension tests attain the peak at lower shear strains compared to compression tests. No consistent difference is observed between the peak stresses in compression and extension with any dissimilarity probably due to a slight lack of sample repeatability accentuated by a shearing ratio that is sub-parallel to the critical state line in the q:p plane. Further experimental evidence is provided later in the paper showing that the slopes of the critical state lines for compression and extension tests are symmetrical about the hydrostatic axis.

Experimental results also suggest that a reduction in slenderness ratio from 2.0 to 1.5 does not have any significant influence on strains uniformity as confirmed by visual inspection of the specimens.

Probing and shearing of specimens after equalization and plastic loading

Figs. 11(a,b,c) compare the results from tests Ba300(-0.5), Bb300(-0.5) and Bc300(-0.5) performed at s=300 kPa on anisotropically compacted specimens subjected to different plastic loading stages with stress ratios [$\Delta q/\Delta p$] =1.2, 0 and -1, respectively, followed by probing with a common stress ratio [$\Delta q/\Delta p$]=-0.5. The purpose of this comparison is to show the effect of the plastic loading ratio on the subsequent behaviour during probing.

For tests Bb300(-0.5) and Bc300(-0.5), the stress ratio of the plastic loading path (i.e. [$\Delta q/\Delta p$] =0 and [$\Delta q/\Delta p$] =-1, respectively) is considerably different from the stress ratio imposed during static compaction (i.e. [$\Delta q/\Delta p$]=1.2). Therefore, in these two tests, a progressive reorientation of particles occurs during plastic loading, which produces a gradual change of stiffness in the v:ln$p$ plane (Fig. 11(c)). Conversely, in test Ba300(-0.5), the stress ratio during plastic loading is identical to that imposed during static compaction so that no reorientation of particles takes place, which results in a sharper change of stiffness in both the q:ε_s and v:ln$p$ planes (Figs. 11(a,c)).

The above interpretation is also consistent with the behavior observed during subsequent probing. The soil exhibits a sharper yielding (Figs. 11(a,c)) as the difference in stress ratio between plastic loading and subsequent probing reduces. For example, a sharper yield point is observed in the q:ε_s plane during probing in tests Bb300(-0.5) and

Bc300(-0.5) (q≈120 kPa and q≈60 kPa, respectively) than in test Ba300(-0.5). As probing progresses beyond yielding, all three tests show an increasingly stiffer response in the q:ε_s plane. This is explained by the low stress ratio during probing which implies a progressive divergence of the soil state from critical state. A typical example of this behaviour is provided by isotropic compression (corresponding to a stress ratio of zero) which produces an increasingly stiffer response if plotted in a linear scale. In the v:ln$p$ plane, the three curves converge towards a single line, which suggests that any fabric difference generated by the distinct plastic loading paths is subsequently erased by the identical stress ratio during probing (Fig. 11(c)).

Fig. 11(a) shows that the increments of shear strain and deviator stress during shearing to failure are very similar for all three tests, though the ratio of the incremental shear strain to volumetric strain shows some differences. In particular, Fig. 11(b) shows that, in tests Ba300(-0.5) and Bb300(-0.5), the specific volume is virtually constant by the time the peak deviator stress is attained but is still decreasing for test Bc300(-0.5). This suggests that the identical stress ratio imposed during probing has erased most fabric history and brought all three specimens to a very similar, though not identical, state before final shearing.

Wetting-induced plastic deformations can also produce an evolution of anisotropy in a similar way to loading-induced plastic deformations. As an example, Figs. 12(a,b,c) compare test Bd100(-0.5), which includes plastic wetting under constant load followed by probing and shearing at s=100 kPa, with test Bb300(-0.5), which includes plastic loading followed by probing and shearing at s=300 kPa (full details of stress paths have been given before). In test Bd100(-0.5), a large compression is observed as soon as suction is reduced from 300 kPa towards 100 kPa, which confirms that the stress state is on the yield surface at the start of wetting. During wetting, a small negative shear strain occurs due to both the anisotropy of soil fabric and the small deviatoric component of the initial stress state. This is similar to the small negative shear strain observed during the isotropic plastic stage of test Bb300(-0.5).

For both tests, the probing path at [$\Delta q/\Delta p$]=-0.5 generates a stiff elastic response in the q:ε_s plane followed, after yielding, by more deformable behaviour and a subsequent further increase in stiffness (Fig. 12(a)). As explained before, the inflection point from softer to stiffer behaviour is typically observed after yielding for stress paths with low stress ratio when plotted in a linear scale.

In terms of volumetric behaviour, Figs. 12(b,c) show that the two specimens exhibit similar values of specific volume at the beginning of probing, which suggests that the different plastic stages have produced similar levels of volumetric hardening and therefore a similar yield surface (this is strictly true only if the elastic strains due to a suction change from 300 kPa to 100 kPa are considered negligible). During probing, the values of specific volume

tend to diverge over an intermediate stress range before becoming similar again towards the end. This is because the probing path of test Bd100(-0.5) was conducted at a lower suction of 100 kPa compared to test Bb300(-0.5), which was instead conducted at a suction of 300 kPa. This means that the former specimen yields at a lower mean net stress, which produces the initial divergence of specific volume. This difference reduces after both specimens have yielded because of the greater stiffness of the virgin compression line at s=100 kPa compared to that at s=300 kPa.

Elastic behaviour

Test A0(0) was repeated on two distinct specimens to explore the elastic behavior of anisotropically compacted specimens during different loading/unloading paths under saturated conditions. The first specimen was subjected to isotropic loading/unloading between the effective stress states of p'=5 kPa, q=1 kPa and p'=300 kPa, q=1 kPa. Subsequently, it was subjected to isotropic loading to p'=150 kPa, q=1 kPa followed by deviatoric loading/unloading to q=75 kPa at constant p'. The second specimen was instead subjected to isotropic loading/unloading/reloading between the two effective stress states of p'=5 kPa, q=1 kPa and p'=100 kPa, q=1 kPa. Subsequently, it was subjected to deviatoric loading/unloading to q=60 kPa at constant p'. An extra unsaturated test, A200(0), involving an isotropic loading/unloading cycle to p=300 kPa, was also performed to explore elastic behavior at s=200 kPa.

Fig. 13 presents the volumetric behaviour observed during the unloading paths of tests A0(0) (both specimens) and A200(0), together with the volumetric behaviour observed during the unloading paths of all plastic loading stages of series Ba300, Bb300, Bc300 and Bd100. Inspection of Fig.13 indicates that swelling lines are approximately parallel for the unsaturated tests at s=300 kPa, s=200 kPa and s= 100 kPa but not for the saturated tests at s=0, which suggests a progressive change of the elastic behaviour as suction reduces towards zero. In addition, the similar slope of all unsaturated swelling lines, regardless of stress ratios, suggests a limited effect of fabric anisotropy on volumetric elastic behaviour. Further experimental evidence is needed to corroborate the above hypotheses. The swelling coefficient with respect to mean net stress was calculated as κ=0.012±0.005 by averaging the slope of all unsaturated swelling lines in Fig. 13.

Elastic deformations due to suction changes were observed during equalization when samples were brought, under a constant small stress, from the suction of 650 kPa after compaction to a suction of either 300 kPa or 100 kPa. The average specific volume after equalization at these two suctions was calculated for both isotropically and anisotropically compacted specimens. Then, the elastic swelling coefficient was calculated from these average

values as κ_s=0.037 by assuming a wetting path from s=300 kPa to s=100 kPa according to the elastic law of the Barcelona Basic Model (Alonso *et al.*, 1990):

$$\Delta v = -\kappa_s \ln \frac{s + \Delta s + p_{atm}}{s + p_{atm}} \tag{1}$$

where Δs is the change of suction and p_{atm} is the atmospheric pressure.

Fig. 14 shows the same experimental data of Fig. 13 but plotted, this time, in the v:ln$p$* plane instead of the v:ln$p$ plane. Even though linearity is considerably less than in the v:ln$p$ plane, in the v:ln$p$* plane all curves can be reasonably fitted by lines with a constant gradient κ*=0.043±0.004. This is true regardless of whether saturated or unsaturated tests are considered, which is one the advantages of using Bishop's stress compared to net stresses.

Another advantage of Bishop's stress is that elastic changes of specific volume can be always related to a change in p* regardless of whether they are produced by a change in net stress or suction. A slightly different value of κ*=0.032 is however obtained if the elastic deformations produced by suction changes during equalization are used in combination with the following elastic equation:

$$\Delta v = -\kappa^* \ln \frac{p^* + \Delta p^*}{p^*} \tag{2}$$

where Δp* is the change of mean Bishop's stress corresponding to the change in suction from 300 kPa to 100 kPa during equalization.

The small difference between the values of κ* obtained from the above two procedures is explained by experimental uncertainties. In particular, the selection of κ* from equalization data is less reliable because it is based on only two values of specific volume, with each value representing the average of multiple tests as explained above.

Fig. 15 shows the unloading paths of the shearing stages of test A0(0) (both specimens) in the q:ε_s plane. It also shows the unloading paths of the plastic loading stages of series Ba300 and Bc300 but not series Bb300 and Bd100 because, in these two cases, the plastic loading stages take place under an isotropic stress ratio. Although elastic behaviour is essentially nonlinear in the q:ε_s plane, the shear modulus is here assumed to be constant, which is acceptable as long as elastic strains are much smaller than plastic strains. A constant value of the elastic shear modulus G=10 MPa was calculated by averaging the slopes of the linear regressions of the unloading curves in the q:ε_s plane (Fig. 15). Some tests exhibit a small increase of shear strain at the beginning of unloading, probably due to delayed straining from previous loading. This portion of the curve was disregarded when calculating the shear modulus.

Critical state

Inspection of Figs. 9 to 12 indicates that values of deviator stress and specific volume are approximately constant over a range of shear strains of 0.05 after the peak deviator stress is attained, which supports the assumption that critical state coincides with peak state. This assumption is further validated in this section by assessing the linearity of the critical state data in the q:p, v:ln$p$, q:p* and v:ln$p$* planes.

Figs. 16(a,b) present critical state data from constant suction triaxial compression and extension tests on both isotropically and anisotropically compacted samples in the q:p and q:p* planes. In the q:p plane, experimental data are interpolated by parallel constant suction lines of slope $\pm M$ (positive or negative sign depends on whether triaxial compression or extension is considered):

$$q = \pm M\left(p + p_s(s)\right) \tag{3}$$

where $p_s(s)$ is the common intercept of the compression and extension lines at suction s.

In the q:p* plane, experimental data are interpolated by two lines covering all suction levels, one line for triaxial compression and another line for triaxial extension (see, for example, Gallipoli *et al.*, 2008). These two lines have equal and opposite slopes $\pm M$* and pass through the origin:

$$q = \pm M^* p^* \tag{4}$$

Experimental data are reasonably interpolated by both equations (3) and (4). Critical states also appear to be independent of initial anisotropy, which might be attributed to the loss of fabric memory during plastic shearing.

Figs. 17(a,b,c,d,e) show critical state data from constant suction triaxial compression and extension tests on both isotropically and anisotropically compacted samples in the v:ln$p$ and v:ln$p$* planes, together with the best fit critical state lines (the normal compression lines at the same suctions from Al-Sharrad (2013) are also shown for reference). At s=100 kPa and s=300 kPa, both isotropically and anisotropically compacted specimens are reasonably interpolated by a single line. This confirms the limited influence of initial anisotropy on critical state, though there is a tendency for the isotropically compacted specimens to lie above the best fit line at low stresses suggesting a slightly steeper critical state slope for these specimens. At zero suction (saturation), the anisotropically compacted specimens tend to exhibit smaller values of specific volume than isotropically compacted ones. The reasons behind this observation remain unclear and will be the object of future investigation.

The equations interpolating critical state data at constant suction in the v:ln$p$ and v:ln$p$* planes are:

$$v_{cs} = \Gamma(s) - \psi(s) \ln p \tag{5}$$

$$v_{cs} = \Gamma^*(s) - \psi^*(s) \ln p^* \tag{6}$$

where $\Gamma(s)$ and $\Gamma^*(s)$ are the intercepts of the critical state lines at suction s while $\psi(s)$ and $\psi^*(s)$ are the corresponding gradients.

Table 2 summarizes the values of all critical state parameters, i.e. M, M^*, $\Gamma(s)$, $\Gamma^*(s)$, $\psi(s)$ and $\psi^*(s)$. In both the v:ln$p$ and v:lnp^* planes, the slopes of the critical state lines decrease with decreasing suction, likewise the normal compression lines.

Yielding and plastic flow

Several methods have been considered in this work to measure the yield stresses and the directions of plastic flow, including those presented by Casagrande (1936), Smith *et al*. (1992), Graham *et al*. (1982), Koskinen *et al*. (2003) and Cui and Delage (1996). The bi-linear method (see Al-Sharrad, 2013) was found to be the best for identifying yield stresses in the v:ln$p$ and v:lnp^* planes because it could be applied to any stress path considered in this study. Due to the difficulty of separating the elastic and plastic components of strain, the direction of plastic flow was calculated by using total strains instead of plastic strains. This is acceptable given that elastic strains are significantly smaller than plastic ones. The direction of the plastic flow vector was therefore obtained by plotting total shear strains ε_s against total volumetric strains ε_v over a small mean net stress increment of 10 kPa starting from the yield point. The gradient of the best-fit line to this plot was taken as the gradient of the plastic flow vector.

The constant suction cross-sections of the yield surface are described in the q:p plane by a distorted ellipse with the following equation:

$$f = \left(q - \alpha\left(p + p_s(s)\right)\right)^2 - m^2\left(p + p_s(s)\right)\left(p_m - p\right) = 0 \tag{7}$$

where $p_s(s)$ is the intersect of the yield ellipse with the negative p axis, which also coincides with the intercept of the critical state line at suction s (see Table 2), m is the ellipse aspect ratio, p_m defines the ellipse size and α defines the ellipse inclination. A schematic plot of the yield curve in the q:p plane is shown in Fig. 18. Alternative forms of distorted or rotated ellipses were considered, including those proposed by Stropeit *et al*. (2008) and D'Onza *et al*. (2010). However, equation (7) was found to give the best match to the measured yield data.

In the q:p^* plane, the constant suction cross-sections of the yield surface are also described by a distorted ellipse but always passing through the origin:

$$f = \left(q - \alpha^* p^*\right)^2 - m^{*2} p^* \left(p_m^* - p^*\right) = 0 \tag{8}$$

where m^* is the ellipse aspect ratio, p_m^* is the ellipse size and α^* is the ellipse inclination. A schematic plot of the yield curve in the q:p^* plane is shown in Fig. 19. This form of yield curve is similar to that suggested by Dafalias (1986) and Wheeler *et al.* (2003) for saturated soils with one difference that the ellipse aspect ratio m^* is independent from the critical state ratio M^*.

A constitutive relationship can be assumed to relate the ellipse aspect ratio, m or m^*, to both the degree of anisotropy, α or α^*, and the critical state ratio, M or M^*. In this way, when the soil approaches critical state, the aspect ratio m or m^* tends towards a limit value that satisfies a zero dilatancy condition if an associated flow rule is assumed. An example of such constitutive relationship can be found in Al-Sharrad (2013).

As a further refinement, different aspect ratios can be assumed for the compression and extension sections of the constant suction ellipses, i.e. for the sections above and below the vertical tangent points. This means that $m=m_c$ for $q/(p+p_s(s))>\alpha$ and $m=m_e$ for $q/(p+p_s(s))<\alpha$ while $m^*=m_c^*$ for $q/p^*>\alpha^*$ and $m^*=m_e^*$ for $q/p^*<\alpha^*$.

Figs. 20(a,b) and Figs. 20(c,d) show the initial yield ellipses of the isotropically and anisotropically compacted specimens after equalization at suctions of zero, 100 kPa and 300 kPa. The experimental fit of equations (7) and (8) is generally good, though measurements are limited to the wet sides of the distorted ellipse. This is because probing ratios larger than 3 or smaller than -1.5 would have required application a tensile radial stress or a tensile axial stress, respectively, which was not possible with the available equipment. In the q:p plane, the compression and extension aspect ratios of the yield ellipses are m_c=0.85 and m_e=1.17, which are noticeably larger than the critical state ratio M=0.752. In the q:p^* plane, the aspect ratios are m_c^*=0.85 and m_e^*=0.95, which are also significantly larger than the critical state ratio M^*=0.672. These aspect ratios are identical for isotropically and anisotropically compacted specimens and remain constant at all levels of suction investigated in this work. Note that these values of aspect ratios are based on a limited number of experimental yield points for each ellipse and further experimental data are needed to confirm the above trends.

The parameters α and α^*, which define the inclination of the distorted yield ellipses in the q:p and q:p^* planes, are equal to zero for isotropically compacted specimens and to α=0.21 and α^*=0.20 for anisotropically compacted specimens. Likewise aspect ratios, the inclinations of the yield ellipses are constant with suction.

Parameters p_m and p_m*, which define the size of the distorted yield ellipses in the q:p and q:p* planes, increase with increasing suction for both isotropically and anisotropically compacted specimens, consistent with existing constitutive models for unsaturated soils (e.g. Alonso *et al.*, 1990). At any suction, the size of the initial yield ellipse (i.e. the yield ellipse after equalization) is bigger for the anisotropically compacted specimens than for the isotropically compacted ones, which is in agreement with the lower initial specific volume of the anisotropically compacted specimens (see Table 1). This confirms the greater volumetric hardening undergone by the soil during sample preparation when subjected to anisotropic compaction compared to isotropic compaction at the same mean net stress.

Series B100bis investigates the behaviour of additional anisotropic specimens statically compacted with the same ratio $[\Delta q/\Delta p]$=1.2 but to a lower mean net stress than other anisotropic specimens, i.e. p=160 kPa instead of p=250 kPa. Because of the lower compaction stress, these specimens have inherited a smaller degree of fabric anisotropy, which corresponds to a smaller initial specific volume (similar to that of isotropic specimens compacted to p=250) and a lower inclination of the yield ellipse (i.e. α=0.08 and α*=0.08) compared to other anisotropic specimens (Figs. 20(e,f))).

Table 3 summarizes the values of aspect ratio (m_c, m_c*, m_e, m_e*), inclination (α, α*) and size (p_m, p_m*) of the constant suction yield ellipses for all tests in Fig. 20.

In series Ba300, Bb300, Bc300 and Bd100, the initial yield surface of the anisotropically compacted samples "evolves" during the intermediate plastic stage. Figs. 21(a,b) show the evolved ellipses for series Ba300, Bb300 and Bc300 together with the initial ellipse from series B300 (dotted line). Inspection of Figs. 21(a,b) confirms that the three intermediate plastic loadings with $[\Delta q/\Delta p]$=1.2, 0 and -1, respectively, produce a change in size and inclination of the yield ellipse. In the q:p plane, the inclination changes from the initial value of α=0.21 to the final value of α=0.29, α=0.19 and α=-0.04 for series Ba300, Bb300 and Bc300, respectively. Instead, in the q:p* plane, it changes from the initial value of α*=0.20 to the final value of α*=0.25, α*=0.12 and α*=-0.10 for series Ba300, Bb300 and Bc300, respectively. Although the same maximum mean net stress is attained in all three plastic loading stages, the size of the yield curve is larger in series Ba300 and Bc300 than in series Bb300, as confirmed by the higher values of p_m and p_m* (see Table 3). This indicates, once again, that an anisotropic stress path results in larger volumetric hardening than an isotropic stress path to the same level of mean net stress.

In series Bd100, plastic wetting from s=300 kPa to s=100 kPa reduces the inclination of the yield ellipse from the initial values of α=0.21 and α*=0.20 to the final values of α=0.19 or α*=0.12 (Fig. 21). These values are identical

to those in series Bb300 (see Table 3), which is consistent with the fact that the imposed stress ratio and the measured deformations are similar during the plastic stages of these two series, as discussed previously.

Inspection of Figs. 20 and 21 indicates that the plastic flow vectors tend to be normal to the yield curves, although some exceptions can be identified. On the basis of these results, the assumption of an associated flow rule appears reasonable if a distorted yield ellipse is assumed. Evidence of normality of flow vectors from past experimental works has however been rather inconclusive. For example, Graham *et al.* (1983) showed that plastic flow vectors are nearly normal to the experimental yield curve of Winnipeg natural clay. On the other hand, Cui and Delage (1996) showed that plastic flow vectors tend not to be normal to the rotated yield ellipse measured in their work.

4. Conclusions

This work investigates the evolution of anisotropy in unsaturated soils with reference to mechanical behaviour. A large number of compression and extension triaxial tests on isotropically and anisotropically compacted specimens have been conducted to investigate yielding and critical state behaviour under a variety of stress paths.

Anisotropically compacted specimens present distorted yield ellipses in the constant suction q:p and q:p^* planes, with a constant inclination at different suction levels. The inclination is relatively small (i.e. α=0.21 and α^*=0.20 in the q:p and q:p^* planes respectively), which is consistent with the small value of Bishop's stress ratio (i.e. $\eta^*=q/p^*\approx0.5$) at the end of compaction suggesting a moderately anisotropic fabric. Experimental results can be interpreted in terms of both net stress and Bishop's stress over a wide range of degrees of saturation from 0.5 to 1. It remains however to be ascertained if Bishop's stress can still be used for degrees of saturation lower than this.

The initial anisotropy is modified by plastic deformations produced by either loading or wetting. Isotropically and anisotropically compacted samples, when loaded along the same stress path, tend to converge in the v:ln$p$ and v:lnp^* planes, which suggests that fabric memory is progressively erased by plastic straining. No strong influence of initial anisotropy on critical state is observed, especially for unsaturated specimens.

5. References

Alonso, E. E. Gens, A. & Josa, A. (1990). A constitutive model for partially saturated soils. *Géotechnique* **40**, Number 3, 405-430.

Al-Sharrad, M. (2013) *Evolving anisotropy in unsaturated soils: experimental investigation and constitutive modelling*. PhD. Thesis, University of Glasgow, UK.

Al-Sharrd, M., Wheeler, S. J. & Gallipoli, D. (2012). Influence of anisotropy on yielding and critical states of an unsaturated soil. *Proc. 2nd European Conference on Unsaturated Soils* (Mancuso C., Jommi C., D'Onza, F. (Eds.)), *Napoli, Italy*, 2, 129-136.

Bishop, A. W. and Henkel, D. J. (1962). *The measurement of soil properties in the triaxial test*. 2nd ed. London: William Clowes and Sons Limted.

Casagrande, A. (1936). The determination of the preconsolidation load and its practical significance. *Proc. 1st International Conference on Soil Mechanics and Foundation Engineering. Cambridge*, 3, 60-64.

Cui, Y. J. & Delage, P. (1996). Yielding and plastic behaviour of an unsaturated compacted silt. *Géotechnique* **46**, N0. 2, 291-311.

Dafalias, Y. F. (1986). An anisotropic critical state soil plasticity model. *Mechanics Research Communications* **13**, No.6, 341-347.

D'Onza, F., Gallipoli, D. & Wheeler, S. J. (2011). Effect of anisotropy on the prediction of unsaturated soil response under triaxial and oedometric conditions. *Proc. 5th Inte. Conf. on Unsaturated Soils. Barcelona, Spain*, 2, 787-794.

Della Vecchia, G., Jommi, C. & Romero, E. (2012). A fully coupled elastic–plastic hydromechanical model for compacted soils accounting for clay activity. *International Journal for Numerical and Analytical Methods in Geomechanics*, DOI: 10.1002/nag.1116.

Gallipoli, D., Gens, A., Chen, G. & D'Onza, F. (2008). Modelling unsaturated soil behaviour during normal consolidation and at critical state. *Computers and Geotechnics* **35**, No. 6, 825-834.

Graham, J., Noonan, M. L. & Lew, K. V. (1983). Yield states and stress–strain relationships in a natural plastic clay. *Canadian Geotechnical Journal* **20**, No.3, 502- 516.

Graham, J., Pinkney, R. B., Lew, K. V. & Trainor, P. G. S. (1982). Curve-fitting and laboratory data. *Canadian Geotechnical Journal* **19**, No. 3, 201-205.

Hattab, M. & Fleureau, J. M. (2011). Experimental analysis of kaolinite particle orientation during triaxial path. *International Journal for Numerical and Analytical Methods in Geomechanics* **35**, No.8, 947-968.

Hicher, P. Y., Wahyudi, H. & Tessier, D. (2000). Microstructural analysis of inherent and induced anisotropy in clay. *Mechanics of Cohesive-Frictional Materials* **5**, No. 5, 341-371.

Koskinen, M., Karstunen, M. & Lojander, M. (2003). Yielding of "ideal" and natural anisotropic clays. *In:* Vermeer, P. A., Schweiger, H. F., Karstunen, M. & Cudny, M., eds. *Inter. Workshop on Geotechnics of Soft Soils-Theory and Practice*. *Noordwijkerhout, Netherlands*, 197-204.

Raveendiraraj, A. (2009). *Coupling of mechanical behaviour and water retention behaviour in unsaturated soils.* PhD. Thesis, University of Glasgow, UK.

Romero, E., Gens, A., Lloret, A.& Barrera, M. (2003). Deformation behaviour of anisotropic and isotropic compacted soils due to wetting. *Proc. 3rd Inter. Sym. on Deformation Characteristics of Geomaterials, IS Lyon*, 743-749.

Sharma, R. S. (1998). *Mechanical behaviour of unsaturated highly expansive clays*. PhD thesis, University of Oxford, UK.

Sivakumar, R. (2005). *Effects of anisotropy on the behaviour of unsaturated compacted clay*. PhD. thesis, Queen's University of Belfast, UK.

Sivakumar, V., Sivakumar, R., Boyd, J. & Mackinnon, P. (2010b). Mechanical behaviour of unsaturated kaolin (with isotropic and anisotropic stress history). Part 2: performance under shear loading. *Géotechnique* **60**, No. 8, 595–609.

Sivakumar, V., Sivakumar, R., Murray, E. J., Mackinnon, P. & Boyd, J. (2010a). Mechanical behaviour of unsaturated kaolin (with isotropic and anisotropic stress history). Part 1: wetting and compression behaviour. *Géotechnique* **60**, No. 8, 581–594.

Sivakumar, V. (1993). *A critical state framework for unsaturated soil*. PhD thesis, University of Sheffield, UK.

Smith, P. R., Jardine, R. J. & Hight, D. W. (1992). The yielding of Bothkennar clay. *Géotechnique* **42**, No. 2, 359-362.

Stropeit, K., Wheeler, S. J. & Cui, Y. J. (2008). An anisotropic elasto-plastic model for unsaturated soils. *Proc. of 1st European Conference on Unsaturated Soils, Durham*, Balkema, 625-631.

Wheeler, S. J. & Sivakumar, V. (2000). Influence of compaction procedure on the mechanical behaviour of an unsaturated compacted clay. Part 2: Shearing and constitutive modelling. *Géotechnique* **50**, No. 4, 369-376.

Wheeler, S. J., Näätänen, A., Karstunen, M. and Lojander, M. (2003). An anisotropic elastoplastic model for soft clays. *Canadian Geotechnical Journal* **40**, No.2, 403-418.

Zakaria, I., Wheeler, S. J. & Anderson, W. F. (1995). Yielding of unsaturated compacted kaolin. *Proc. of the 1st Inter. Conf. on Unsaturated Soils, Paris*, Rotterdam, Balkema, 1, 223-228.

TABLES

Table 1. Specimens properties

Test series	*s*, kPa	As-compacted				After suction equalization		
		w	*v*	*Sr*	Initial dry density (g/cm^3)	*w*	*v*	*Sr*
A300	300	0.2470 (±0.0012)	2.317 (±0.014)	0.4875 (±0.0045)	1.122 (±0.007)	0.2812 (±0.0055)	2.345 (±0.012)	0.5435 (±0.0078)
A100	100					0.3639 (±0.0043)	2.360 (±0.015)	0.6951 (±0.0134)
A0 (saturated)	0							
B300 Ba300 Bb300 Bc300 Bd100	300	0.2474 (±0.0015)	2.169 (±0.009)	0.5501 (±0.0053)	1.199 (±0.005)	0.2802 (±0.0049)	2.185 (±0.008)	0.6147 (±0.0108)
B100	100					0.3612 (±0.0044)	2.214 (±0.008)	0.7729 (±0.0135)
B0 (saturated)	0							
B100bis	100	0.2465 (±0.0008)	2.319 (±0.018)	0.4857 (±0.0079)	1.121 (±0.009)	0.3658 (±0.0036)	2.363 (±0.016)	0.6976 (±0.0123)

Table 2. Critical state parameter values

s, kPa	*M*	$p_s(s)$, kPa	$\psi(s)$	$\Gamma(s)$	*M**	$\psi^*(s)$	$\Gamma^*(s)$
300	±0.752	154	0.187	2.961	±0.672	0.341	4.046
100		67	0.128	2.614		0.196	3.058
0		0	0.123	2.575		0.123	2.575

Table 3. Parameter values of yield curves in the *q*:*p* and *q*:*p** planes

Test series	*q*:*p* plane				*q*:*p** plane			
	m_c	m_e	α	p_m (kPa)	m_c^*	m_e^*	α^*	p_m^* (kPa)
A300	0.85	1.17	0	104	0.85	0.95	0	244
A100			0	42			0	101
A0			0	15			0	16
B300			0.21	141			0.20	300
B100			0.21	54			0.20	122
B0			0.21	22			0.20	23
Ba300			0.29	268			0.25	468
Bb300			0.19	215			0.12	398
Bc300			-0.04	266			-0.10	470
Bd100			0.19	98			0.12	179
B100bis			0.08	39			0.08	99

FIGURES

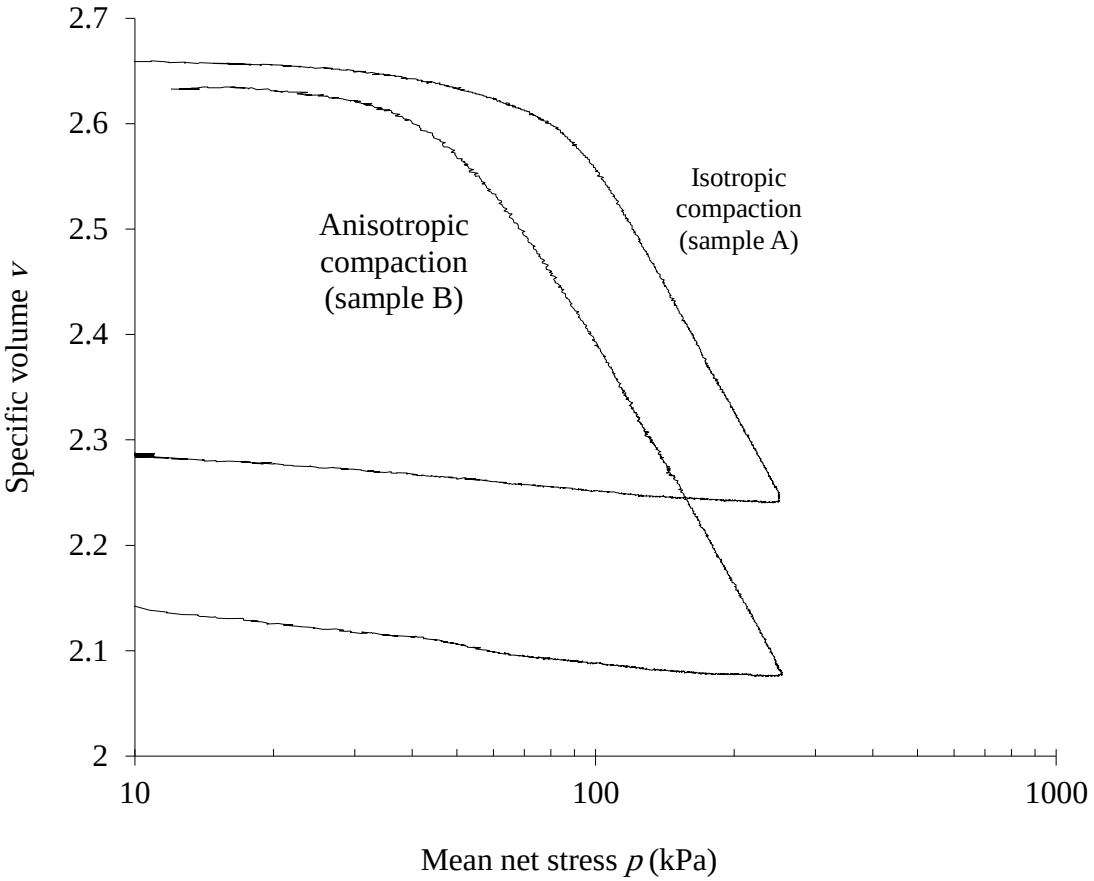

Figure 1. Compression behaviour during isotropic and anisotropic compaction

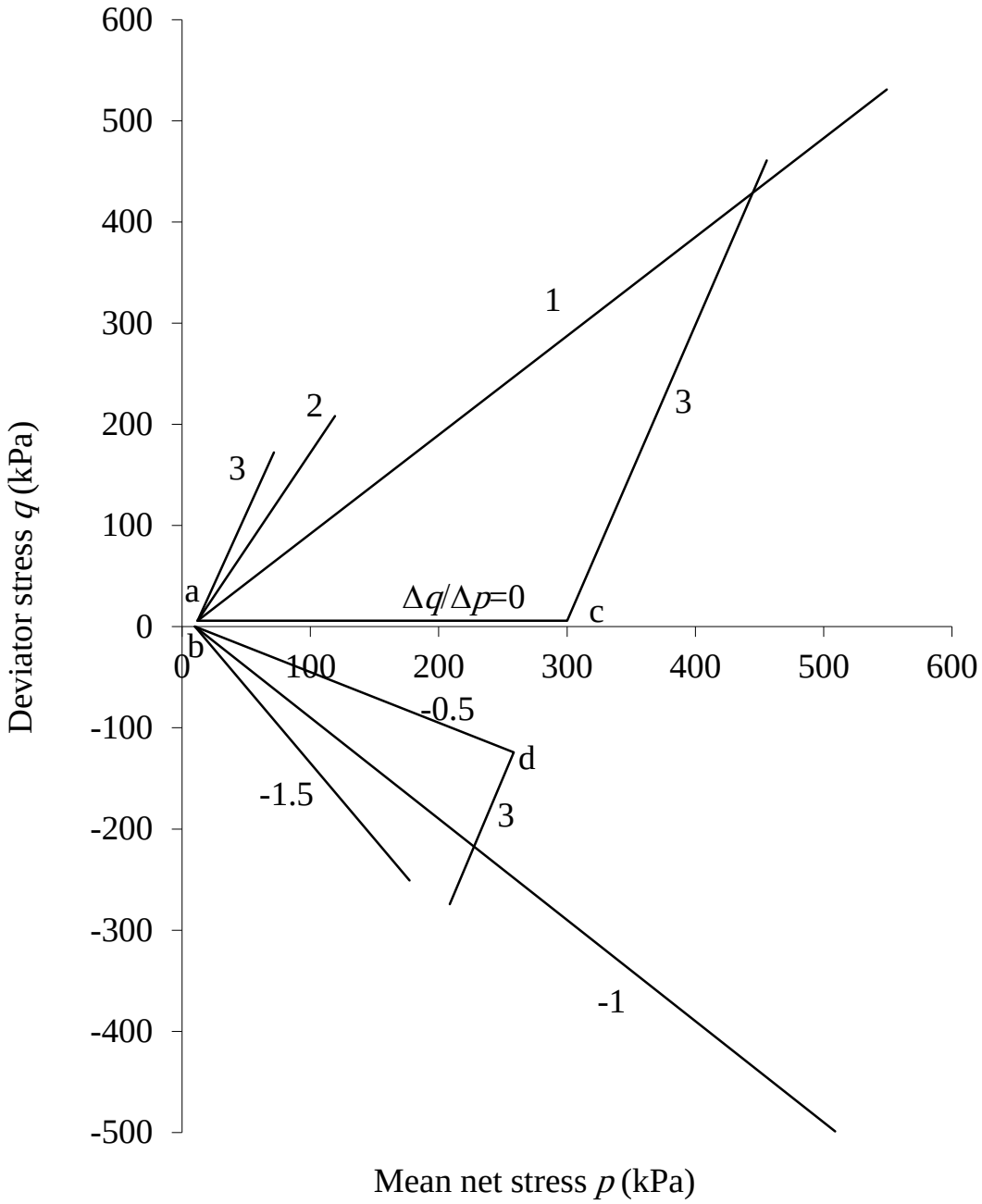

Figure 2. Stress paths of test series A100, A300, B100, B300 and B100bis (note that test series B100bis does not include probing at $\Delta q/\Delta p=3$)

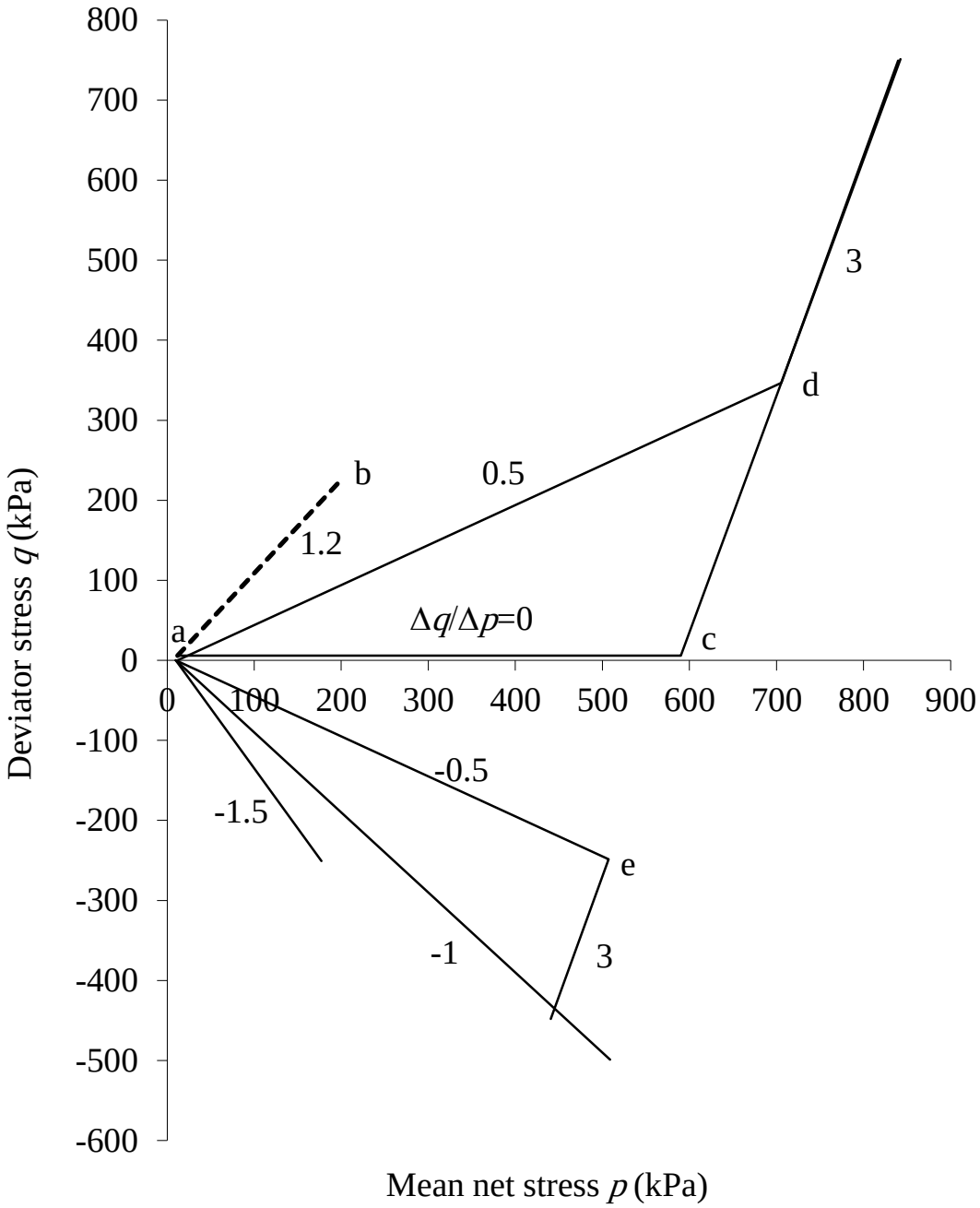

Figure 3. Stress paths of test series Ba300

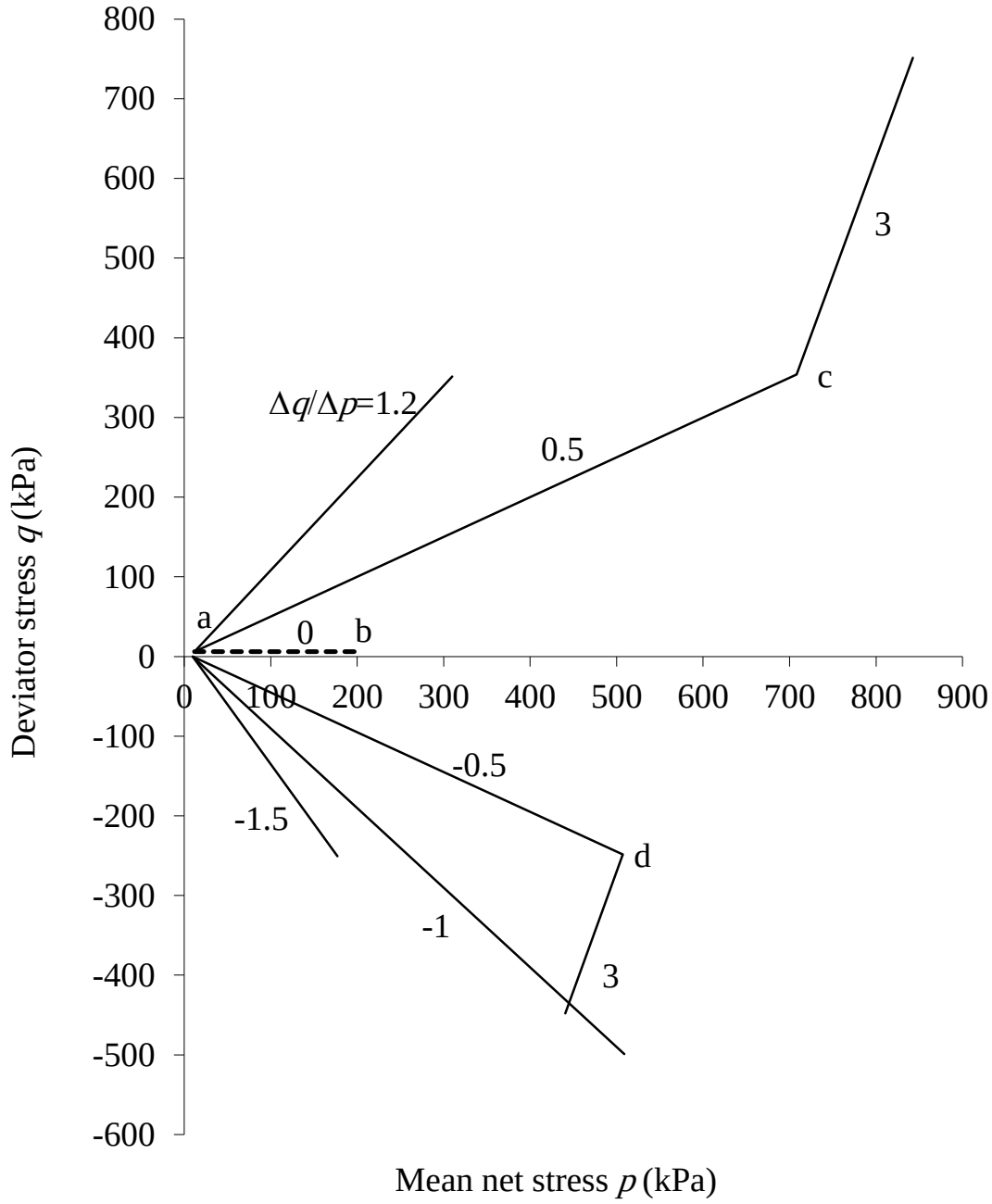

Figure 4. Stress paths of test series Bb300

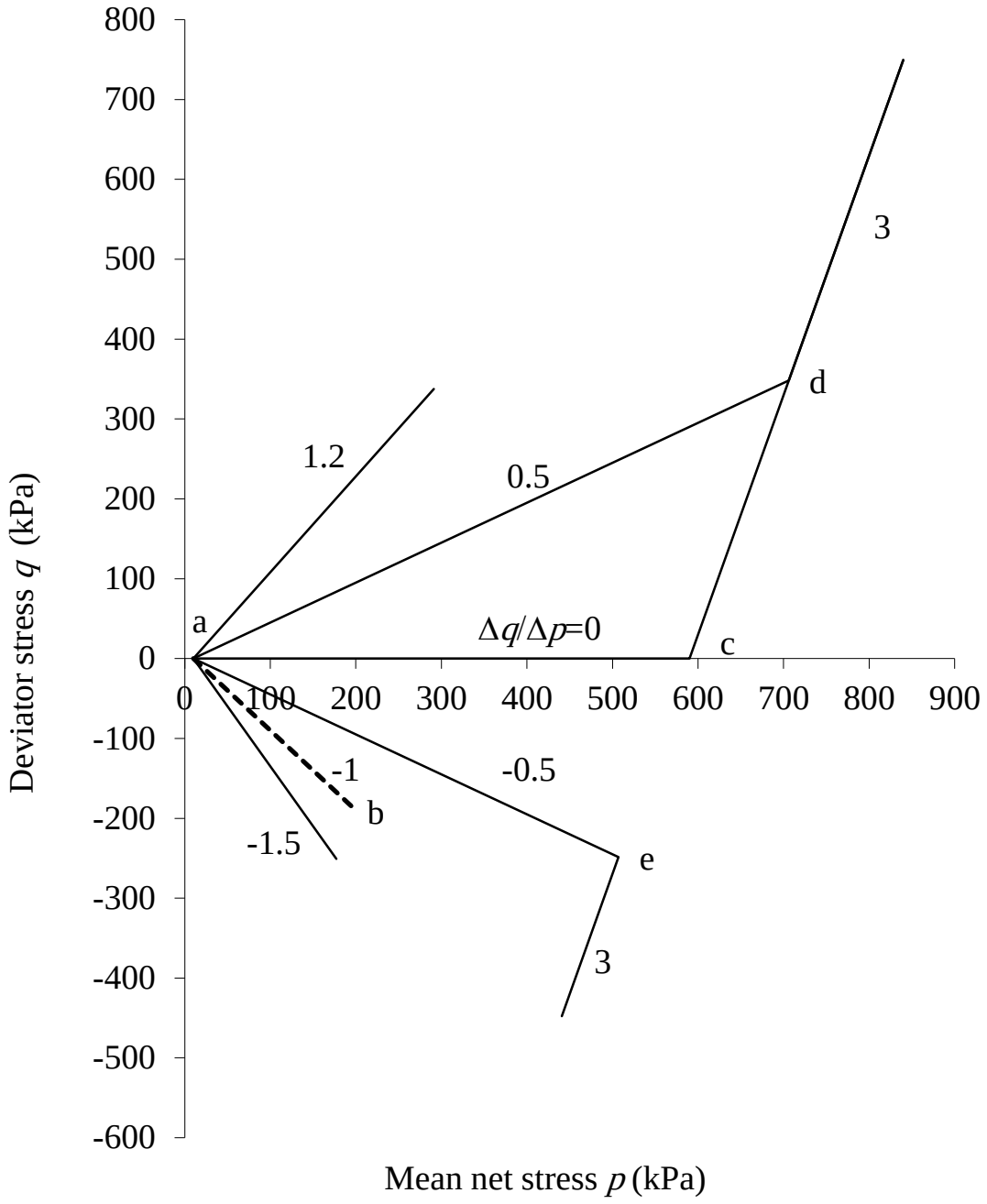

Figure 5. Stress paths of test series Bc300

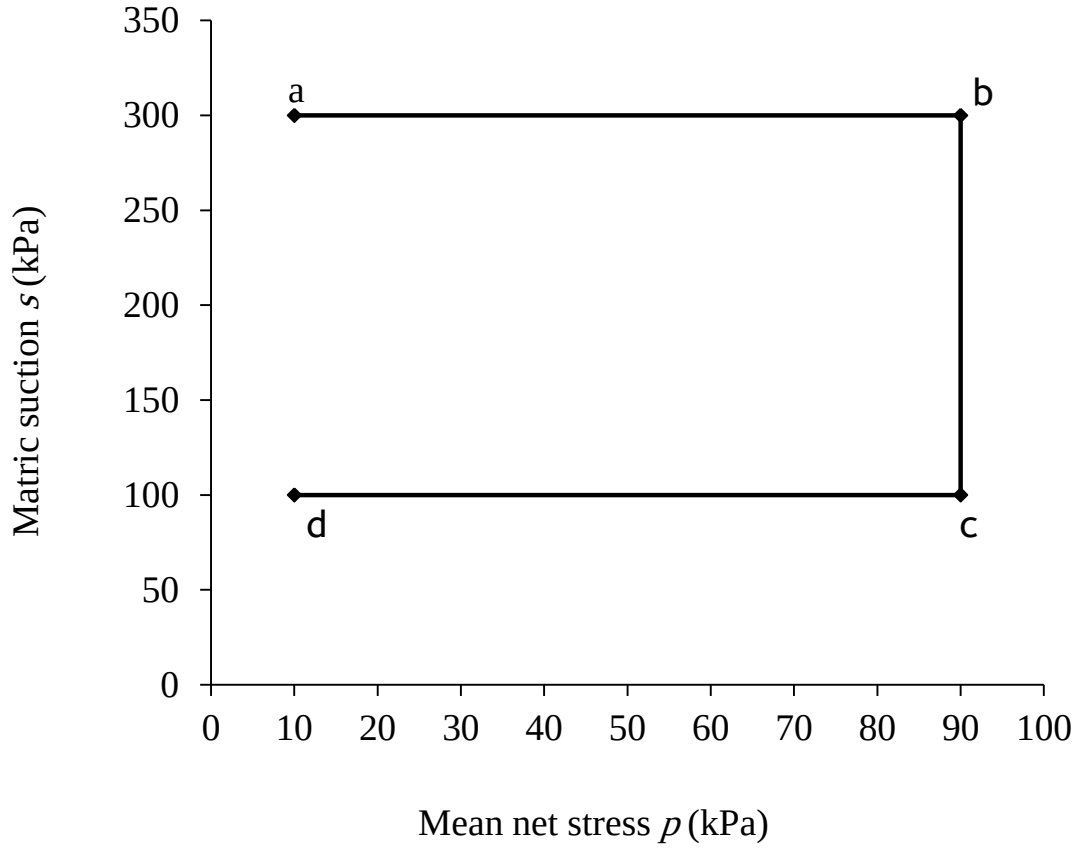

Figure 6. Loading, wetting and unloading stages in series Bd100

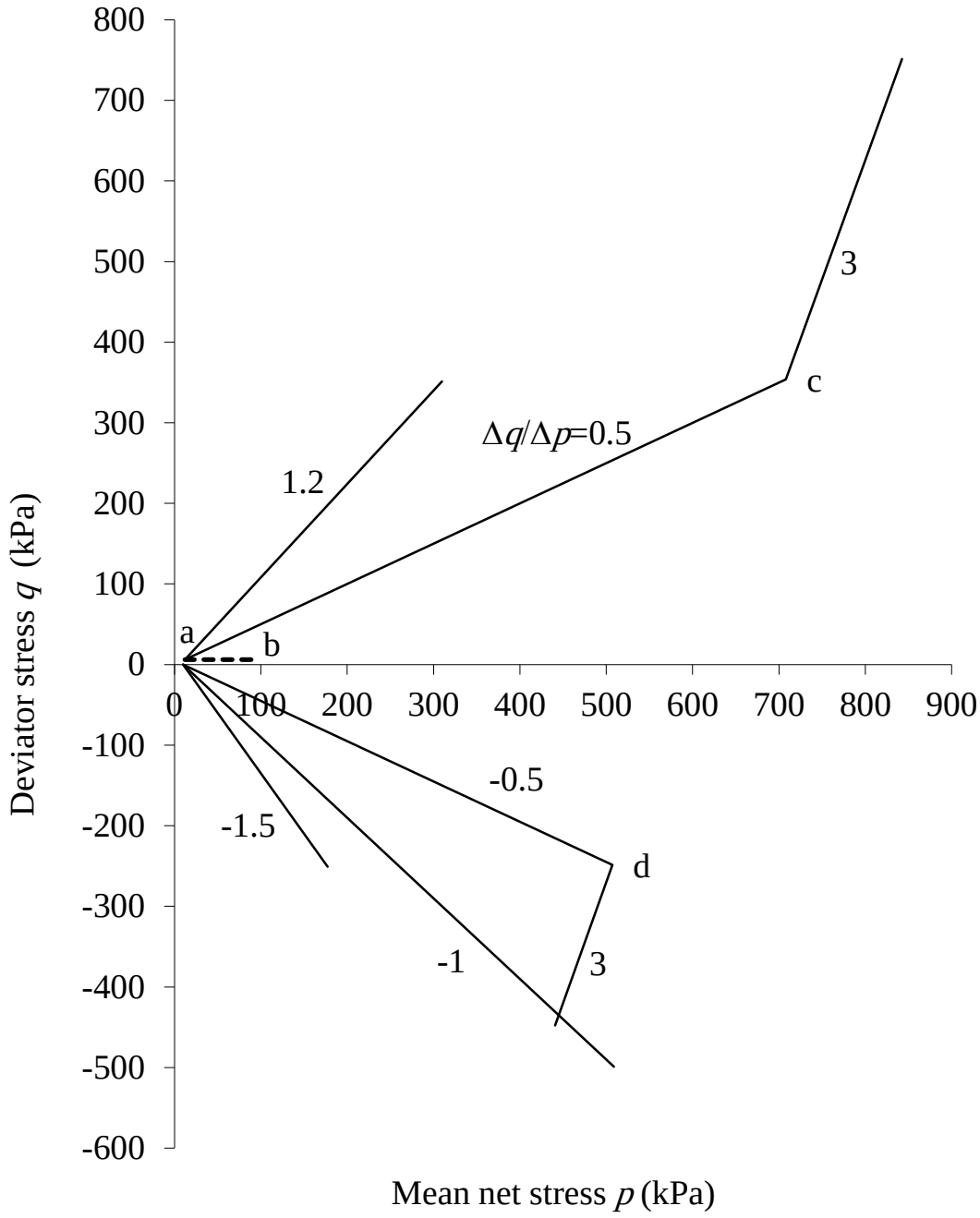

Figure 7. Stress paths of test series Bd100

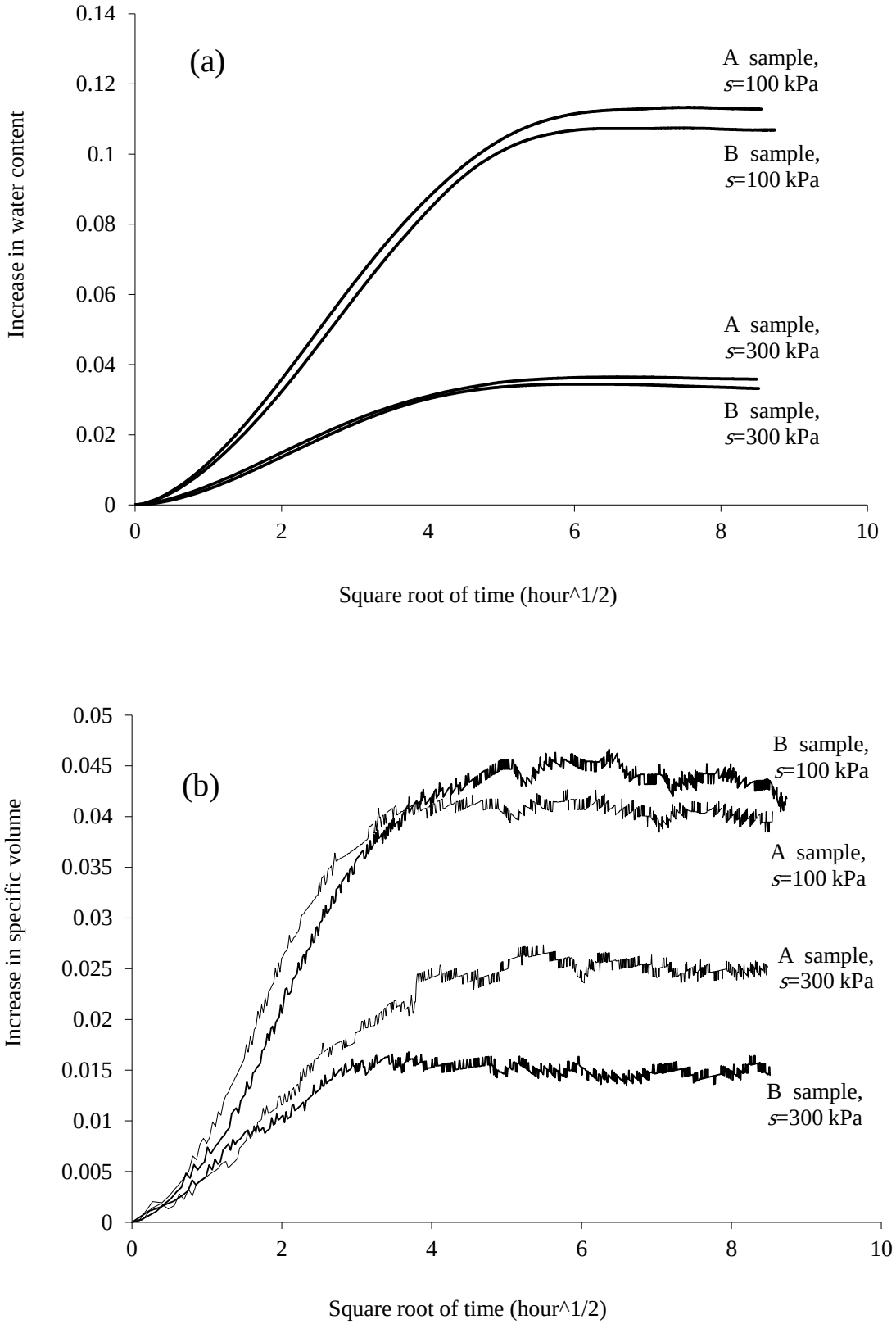

Figure 8. Typical results from equalization stages for isotropically compacted samples (A samples) and anisotropically compacted samples (B samples)

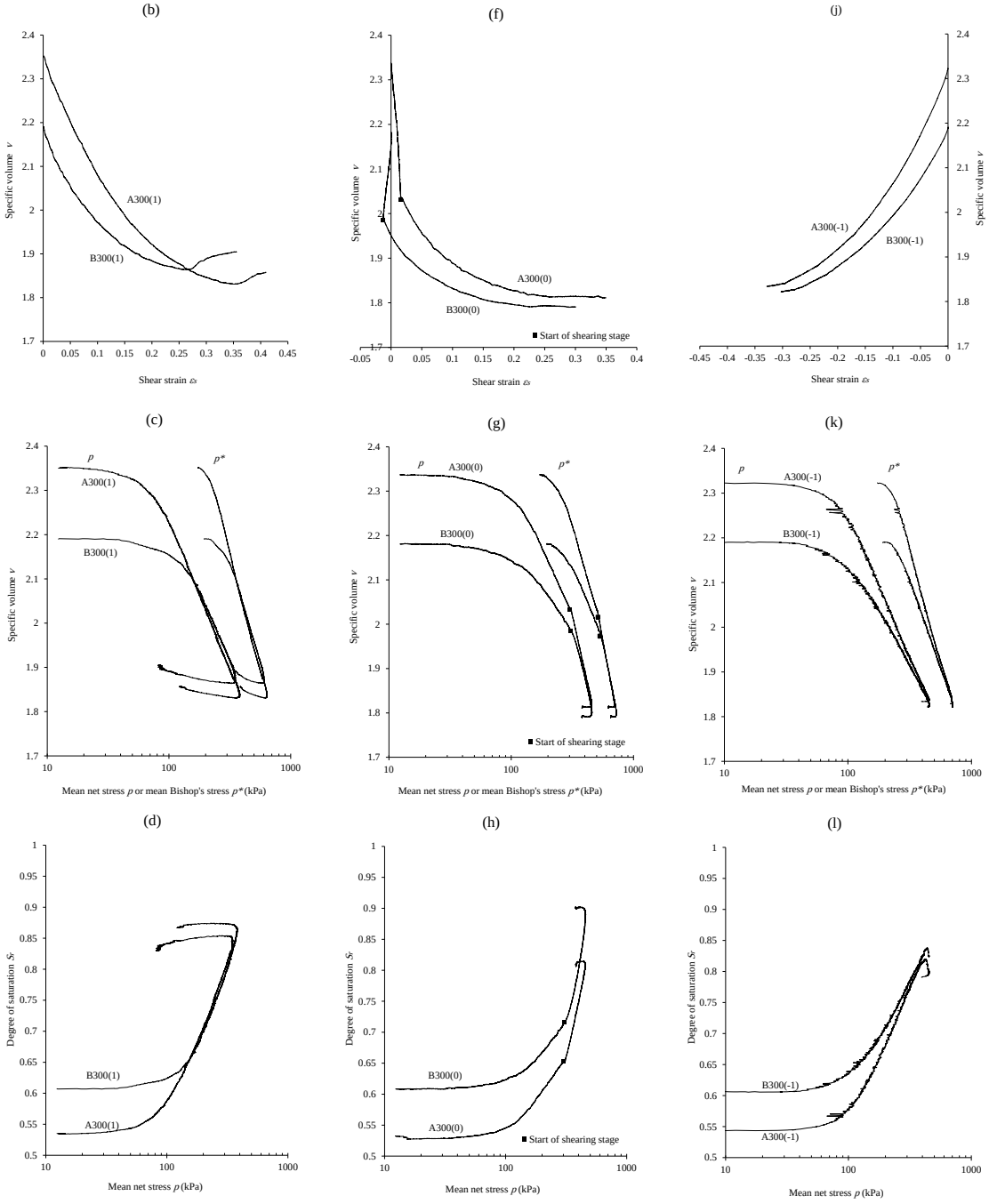

Figure 9. Probing and shearing behaviour of isotropically and anisotropically compacted specimens

(a)

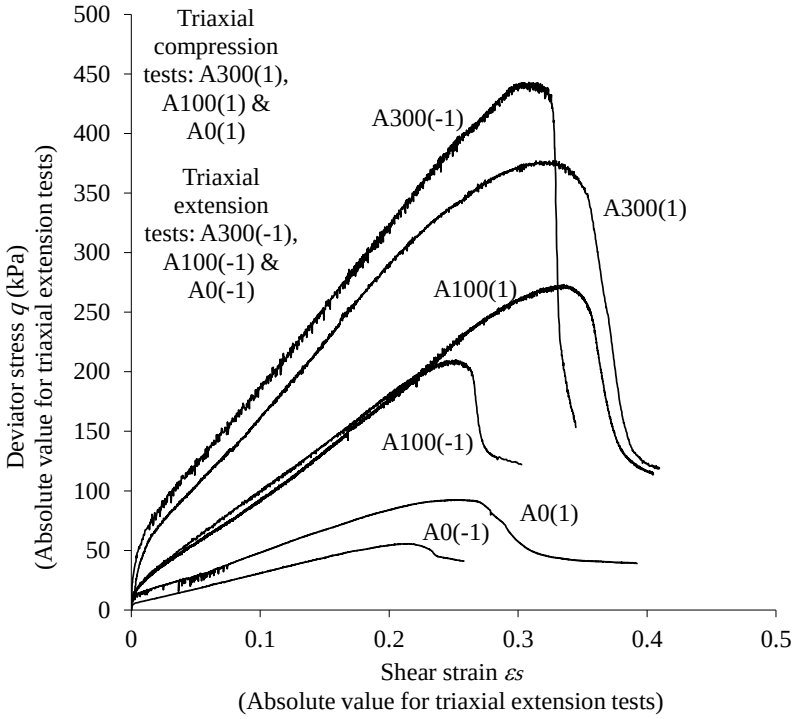

(b)

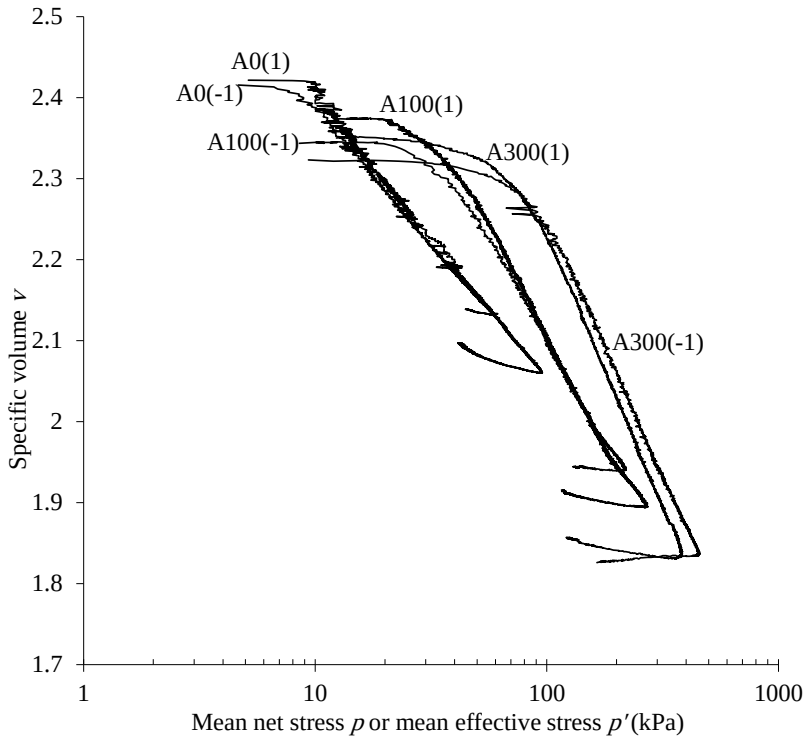

Figure 10. Probing behaviour of isotropically compacted specimens in triaxial compression and extension

(a)

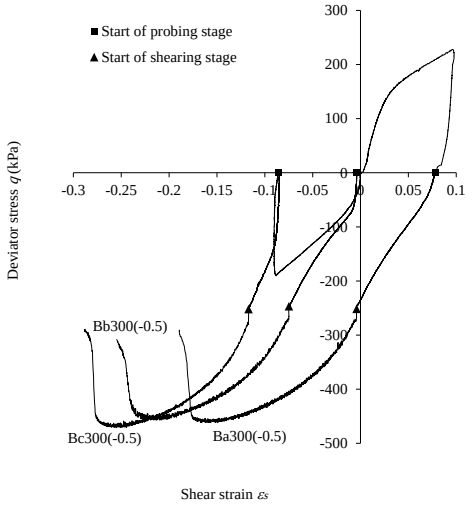

(b)

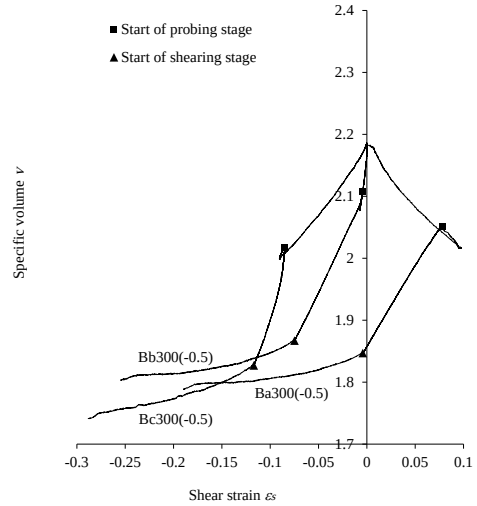

(c)

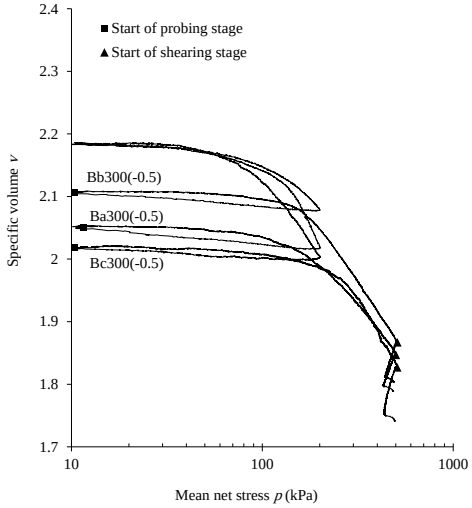

Figure 11. Probing and shearing behaviour of anisotropically compacted specimens subjected to prior plastic loading

(a)

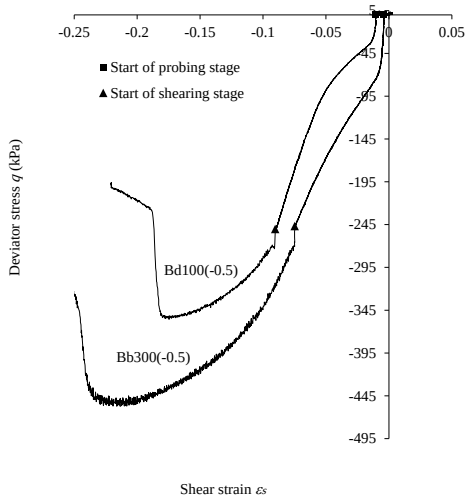

(b)

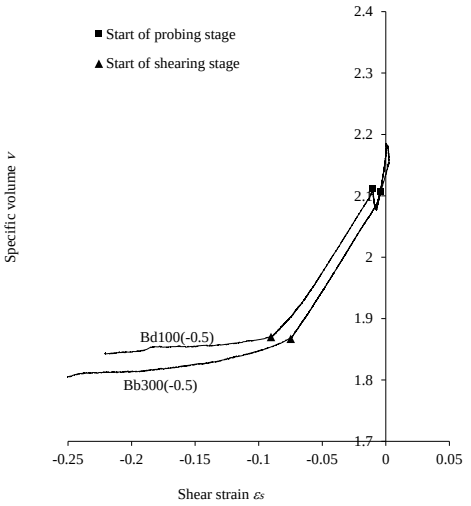

(c)

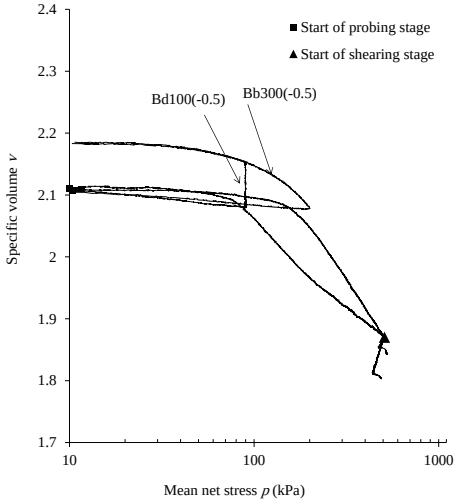

Figure 12. Probing and shearing behaviour of anisotropically compacted specimens subjected to prior plastic loading or wetting

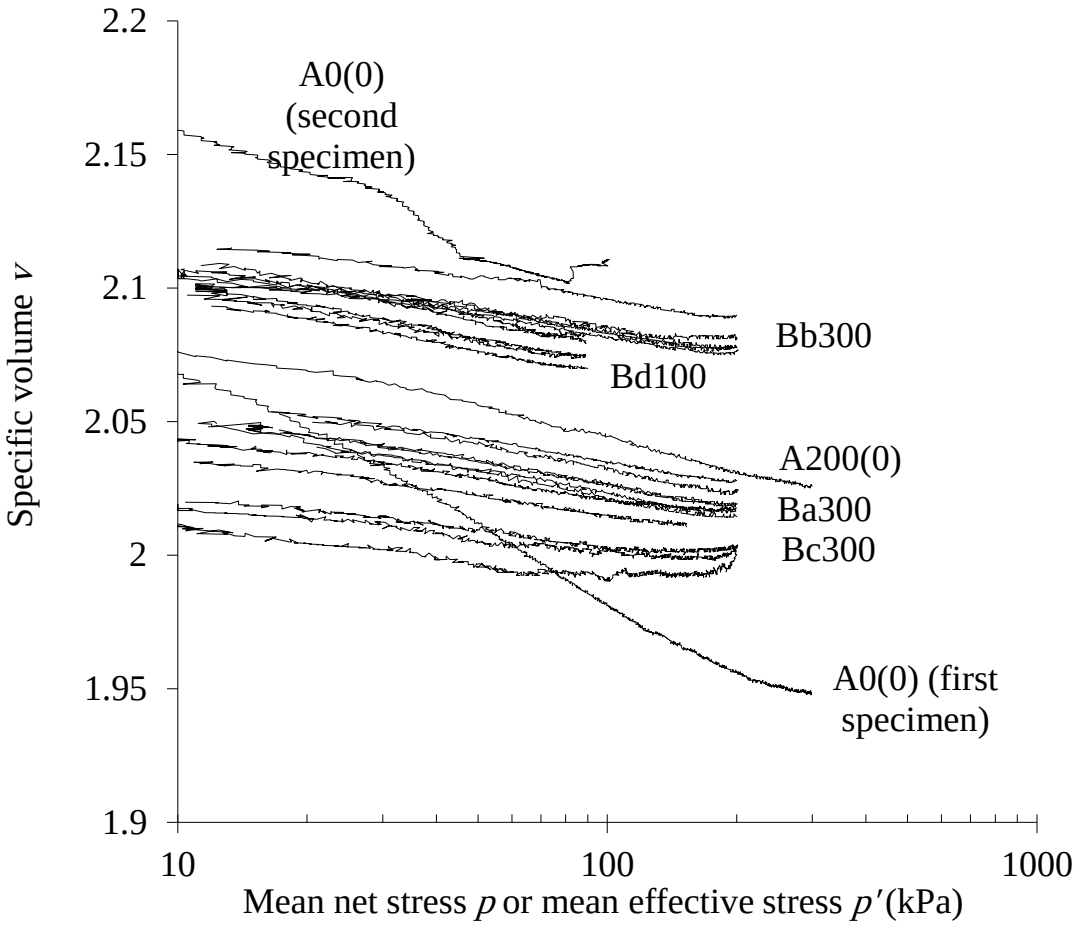

Figure 13. Elastic swelling of specimens with variable anisotropy during constant suction unloading in the *v*:ln*p* or *v*:ln*p'* planes

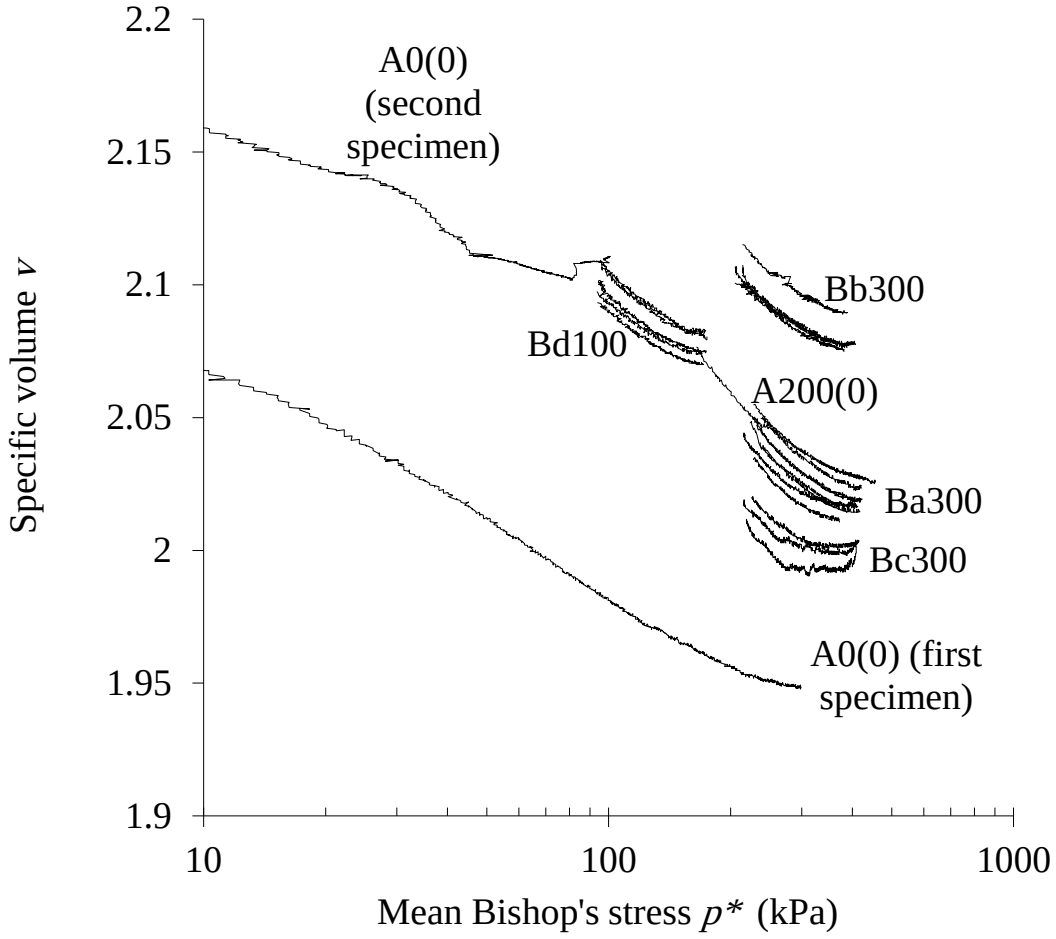

Figure 14. Elastic swelling of specimens with variable anisotropy during constant suction unloading in the v:ln$p$* plane

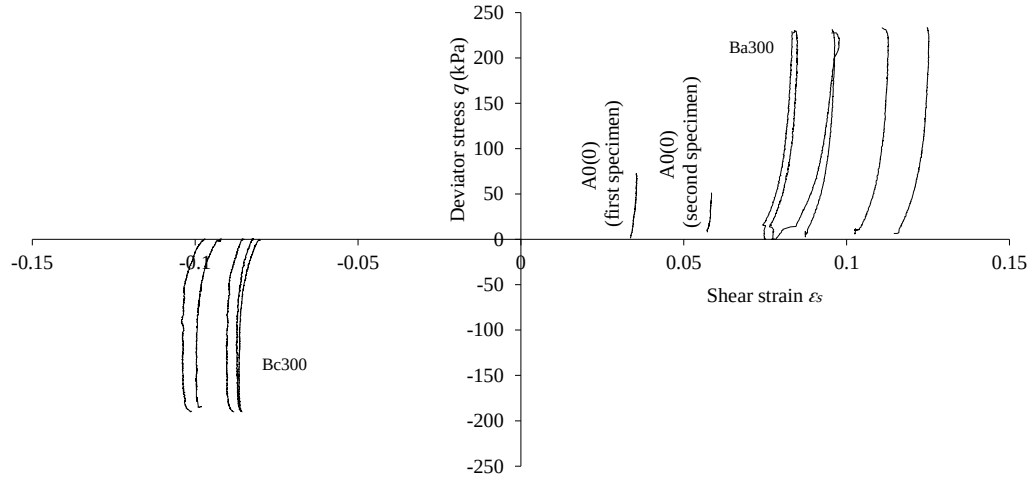

Figure 15. Elastic shear deformation of specimens with variable anisotropy during constant suction unloading in the q:ε_s plane

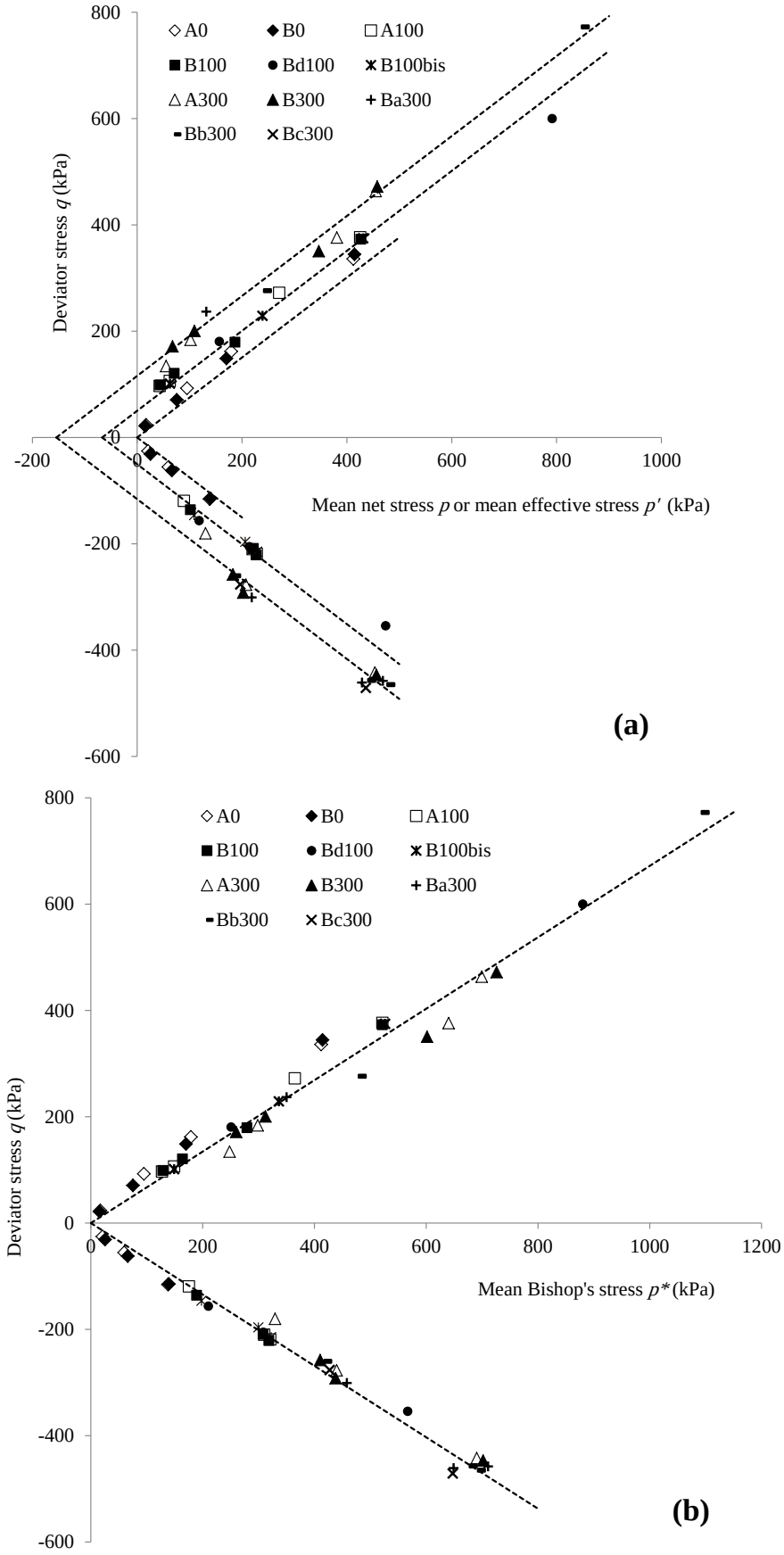

Figure 16. Critical states of isotropically and anisotropically compacted samples in the: (a) *q*:*p* plane and (b) *q*:*p** plane

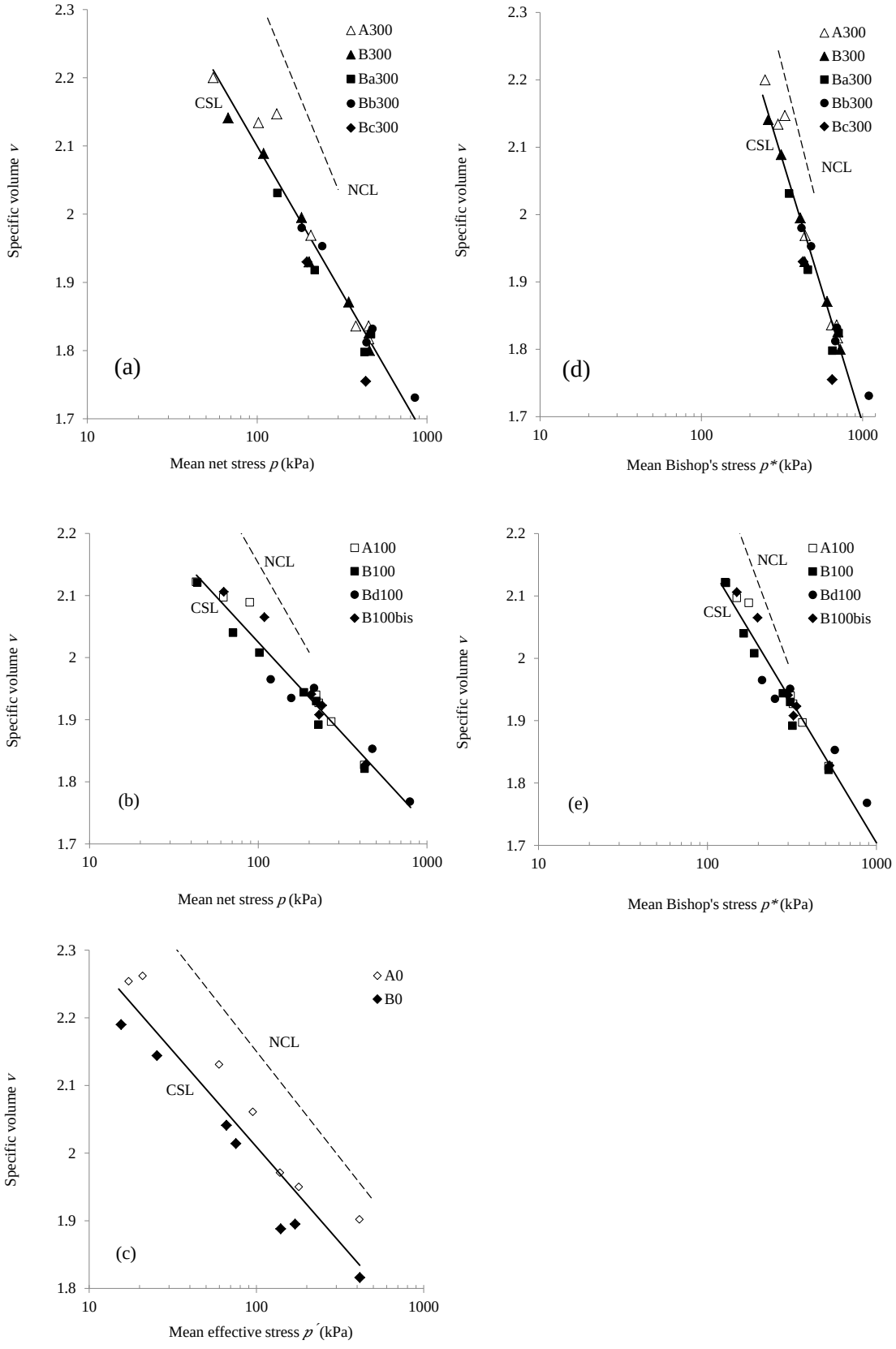

Figure 17. Critical states of isotropically and anisotropically compacted samples in the: (a), (b) *v*:ln*p* plane, (c) *v*:ln*p´* plane and (d), (e) *v*:ln*p** plane

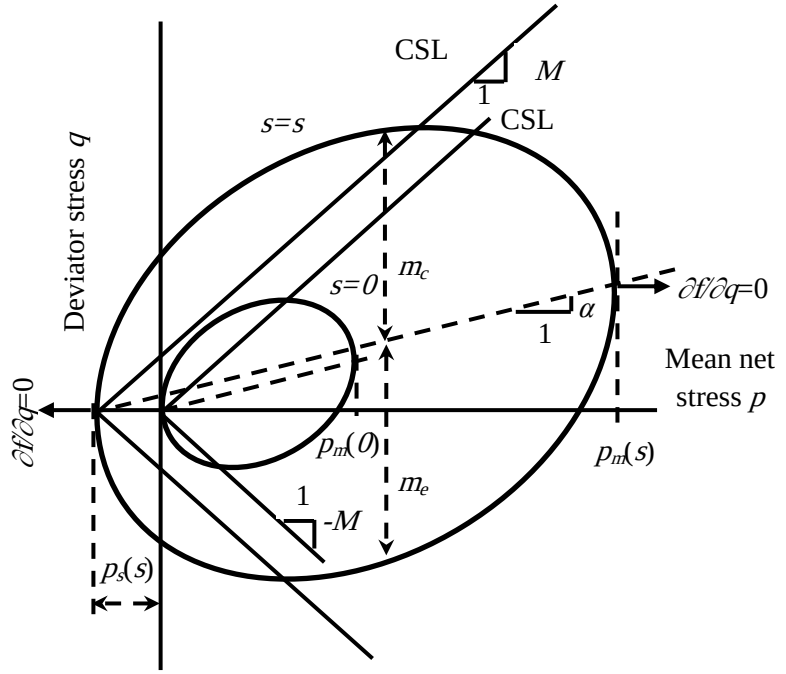

Figure 18. Schematic plot of the constant suction cross-section of the yield surface in q:p plane

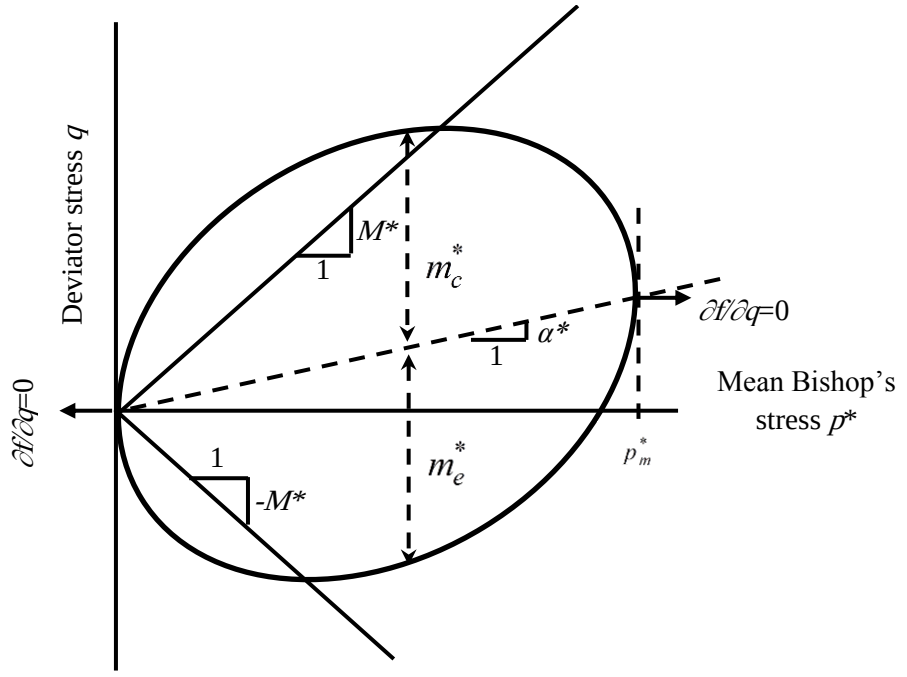

Figure 19. Schematic plot of the constant suction cross-section of the yield surface in q:p^* plane

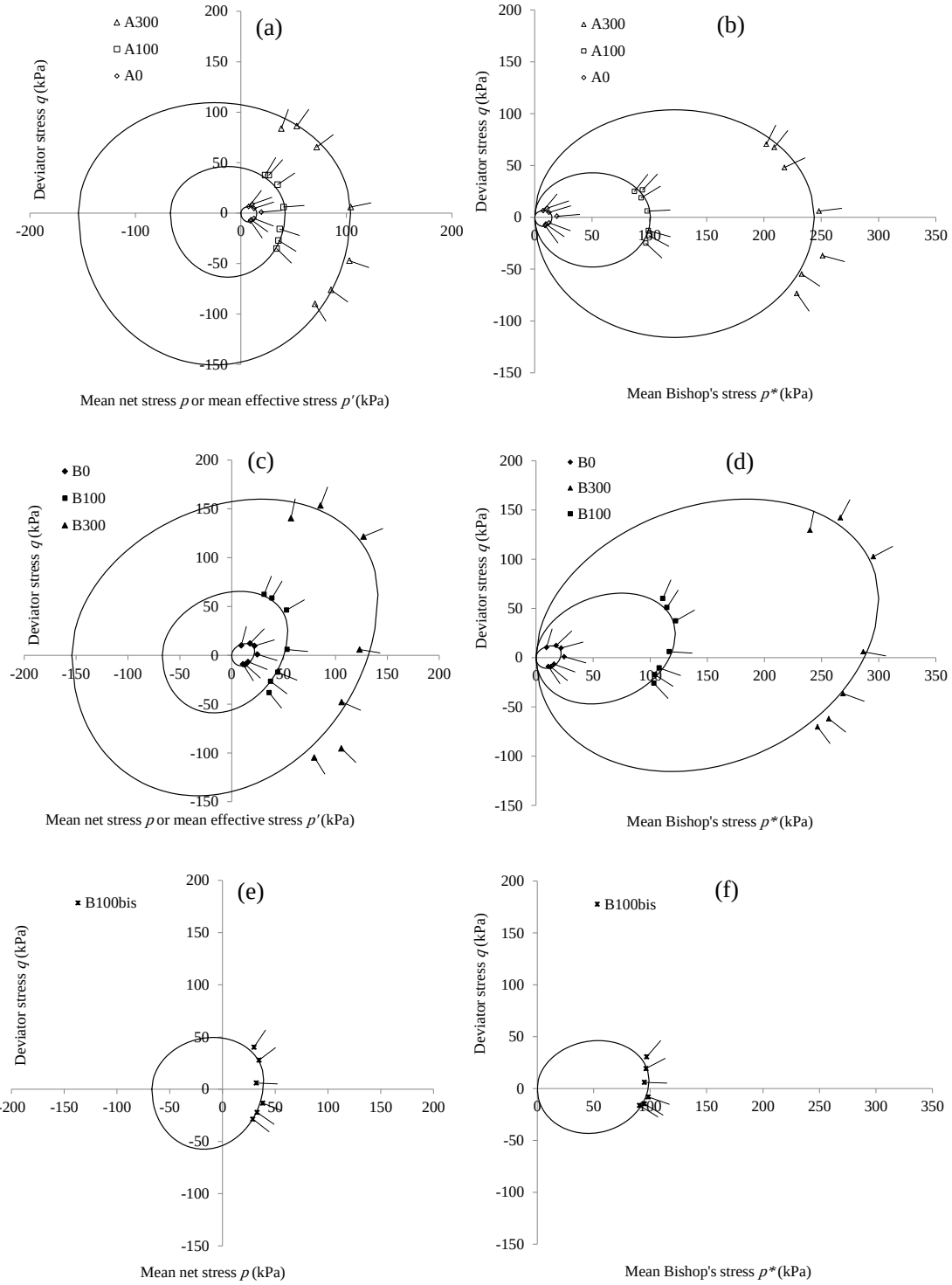

Figure 20. Constant suction cross-sections of initial yield surfaces, together with measured yield stresses and plastic flow vectors, in the *q*:*p* and *q*:*p** planes for: (a)(b) isotropically compacted samples; (c)(d) anisotropically compacted samples; (e)(f) anisotropically compacted samples at higher void ratio (similar void ratio as isotropically compacted samples)

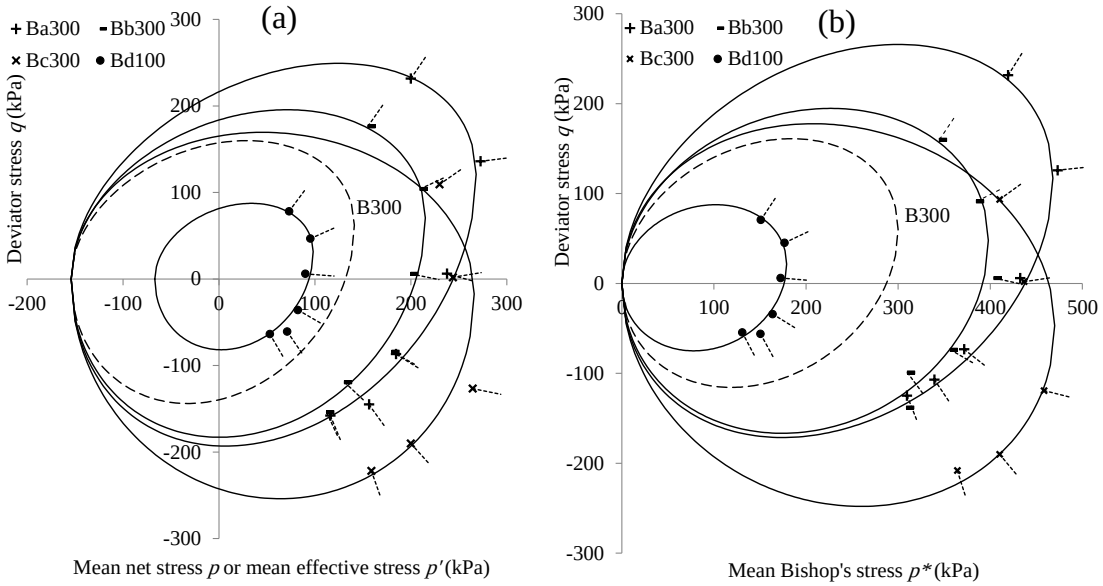

Figure 21. Constant suction cross-sections of evolved yield surface, together with measured yield stresses and plastic flow vectors, in the q:p and q:p^* planes for anisotropically compacted samples subjected to plastic straining at s=300 kPa (dotted line indicates initial yield surface before plastic straining)